Spring 5-1-2013

Vitamin B12-Based Bioconjugate Probes for in Vitro and in Vivo Imaging

Anna Kahkoska

Vitamin B_{12}-Based Bioconjugate Probes for *in Vitro* and *in Vivo* Imaging

A Capstone Project Submitted in Partial Fulfillment of the Requirements of the Renée Crown University Honors Program at Syracuse University

Anna Kahkoska
Candidate for B.S. in Biochemistry
and Renée Crown University Honors
May 2013

Honors Capstone Project in Biochemistry

Capstone Project Advisor: _____
Robert Doyle, Professor

Capstone Project Reader: _____
Cathryn Newton
Professor and Dean Emerita

Honors Director: _____
Stephen Kuusisto, Director

Date: April 24, 2013

Abstract

Cancer is the second leading cause of death in the United States. This year, an estimated 577,190 Americans will die as a result of this family of diseases. Finding cancer at its most treatable stage gives patients the greatest chance of recovery; novel imaging agents that target primary and metastasized tumors offer hope for improved prognoses in the future. Based on the hypothesis that vitamin B_{12} (B_{12}) and its association with specific transport proteins could offer selective access to cancer cell lines, a series of B_{12}-based imaging agents were synthesized, characterized, and assayed for both *in vitro* and *in vivo* functions. A water soluble B_{12}-Re(I) probe that incorporated the thiazole linker-chelator moiety was used to demonstrate the presence of cubilin in A549 lung cancer cells, and a B_{12}-^{64}Cu probe was shown to selectively target tumor cells through specific receptors for B_{12} in a mouse model. These findings suggest that B_{12}-based bioprobes have great promise for cancer cell lines *in vitro* and targeting tumors as imaging agents *in vivo*. The remarkable B_{12} bioprobes developed here have a future as tools to better understand the biochemistry of B_{12} specifically and the physiology of cancer more generally, a fascinating interface of two discrete fields of study.

Table of Contents

Preface

Diseases desperate grown
By desperate appliance are relieved,
Or not at all.

(From William Shakespeare's Hamlet, Act IV, Scene III)

Acknowledgements

This work has been funded by the iLearn Undergraduate Research Program grant, the Crown-Wise Award from the Renée Crown University Honors Program, and the American Cancer Society. It would not have been possible without collaboration with Dr. Mette Madsen at the University of Aarhus and Dr. Tayo F. Ikotun and Prof. Suzanne Lapi in the Dept. of Radiology at Washington University. I would like to thank the Doyle group for being so knowledgeable, patient, and supportive. Amy Rabideau, Dr. Tony Vortherms, and Dr. Chris Fazen helped with the research for this project, and Professor Cathryn Newton read the manuscript. Finally, I would like to thank Professor Robert Doyle for his all-encompassing mentorship over the last four years.

1 Project Overview

The overarching goal of this research was to synthesize imaging agents that selectively target tumor cells through specific receptors for vitamin B_{12} (B_{12}). B_{12} is essential for cellular metabolism, growth, and division, and all living cells require it for survival.[1] Mammals cannot synthesize B_{12}, so they must obtain it through the diet. As a result, the human body has developed a complex dietary uptake system based on soluble transport proteins in the mouth (haptocorrin, HC), intestine (intrinsic factor, IF) and circulatory system (transcobalamin II, TCII).[2]

The construction of the B_{12}-based probes presented in the future chapters was based on the hypothesis that the B_{12} pathway can be exploited to offer a tropism for cancer cells, due to the fact that certain cancer cell lines overexpress uptake receptors for TCII (CD320 receptors) in order to meet the increased B_{12} demands of their rapid and uncontrolled growth. In addition, it was recently discovered that some cell lines, like those of pancreatic cancer, express membrane-bound HC *de novo*. This HC finding has great potential for an even more specific targeting of cancer cells.

The specific aims were to synthesize, characterize, and assay a series of B_{12}-based imaging agents for both *in vitro* and *in vivo* functions, including a fluorescent B_{12}-based probe with which to screen cell lines for receptor targets and a radiolabeled B_{12}-based probe with which to target tumors in living organisms.

2 Cancer

2.1 Pathology

Cancer, or malignant neoplasm, describes not just one disease, but a host of diseases marked by unrestrained proliferation of abnormal cells.[3] Unlike regular cells, which undergo scheduled differentiation and apoptosis, cancer cells divide uncontrollably, invade normal tissues, and may metastasize to other tissues and organs.3 The mechanisms by which cells become cancerous are genetic and environmental; cancer is thought to occur by DNA mutations which inhibit normal cell signaling and apoptosis. Cancer can occur in nearly every tissue in the body, and different types of cancers are clinically treated as distinct diseases; each is associated with unique risk factors, prognoses, and treatments.[4] Prostate cancer, breast cancer, lung cancer, colorectal cancer, and melanoma are prevalent in the US today.[5]

While the epidemiology of cancer is complex to study, it has been shown that viral infections such as infection by human papilloma virus[6], environmental factors such as UV radiation from the sun,[7]and lifestyle factors such as smoking tobacco[8] are associated with the development of cervical cancer, skin cancer, and lung cancer, respectively. In order to resolve the genetic mechanisms of cancer, scientists are focused on sequencing the cancer genome to identify particularly high-risk mutations that contribute to cancer development and recurrence.[9]

2.2 Epidemiology

The American Cancer Society estimates that 577,190 Americans are expected to die as a result of cancer in 2013.4 In 2012, cancer was cited as the second leading cause of death in the US.5 Based on rates from 2007-2009, 41.24% of men and women born today will be diagnosed with a form of cancer at some point during their lifetime.5

However, trends in epidemiology reflect advances in the field that allow physicians to diagnose and treat cancer more effectively; over the past three decades, the 5-year survival rate patients diagnosed with cancer has improved from 49% to 67%.4 The NCI emphasizes that finding cancer at its most treatable stage gives patients the greatest chance, yet, there is still a great need for enhanced methods of detection, early or otherwise.4 Currently, tumors are most often detected via blood-work, X-rays, computed tomography scans, magnetic resonance imaging scans, and positron emission tomography scans.[10]

Finding novel imaging agents that selectively highlight primary and metastasized tumors could radically improve cancer survival rates by permitting better diagnoses and earlier intervention. This capstone project identifies new and important imaging techniques using B_{12}.

2.3 Metastasis

Metastasis refers to the spread of cancer from the site of a malignant tumor in one part of the body to other organs or tissues.[11] Commonly, a piece of the original tumor, termed the primary tumor, breaks away and enters the bloodstream or lymphatic system, which circulates these cells to a different part of the body via hematogeneous or lymphatic spread, respectfully.[12] These cells can form a tumor in a new site, termed the metastatic tumor. Because the metastatic tumor is composed of cells from the primary tumor, it retains markers or antigens on the cell surface that can be used to indicate the primary site of the cancer.[13] There are certain patterns of metastasis that are well-characterized (Table 2.1).[12] The most common sites of metastasis from solid tumors are the lungs, bones, liver, and brain.[13]

Cancer type	Common sites of metastasis
Breast	Lungs, liver, bones
Colon	Liver, peritoneum, lungs
Kidney	Lungs, liver, bones
Lungs	Adrenal gland, liver, lungs
Melanoma	Lungs, skin/muscle, liver
Ovary	Peritoneum, liver, lungs
Pancreas	Liver, lungs, peritoneum
Prostate	Bones, lungs, liver
Rectum	Liver, lungs, adrenal gland
Stomach	Liver, peritoneum, lungs
Thyroid	Lungs, liver, bones
Uterus	Liver, lungs, peritoneum

Table 2.1.Common Metastasis Sites by Cancer Type.

Metastatic cancers are particularly problematic because they are difficult to detect and diagnose. Once circulated, metastatic cancer cells can lie dormant for long periods of time before growing into a clinically detectable tumor, and

metastatic disease may be found before, at the same time as the primary tumor, or much later.[12] If the metastatic tumor is detected first, it is characterized and used to identify the primary cancer. As with primary tumors, therapy for metastatic cancer usually involves chemotherapy, radiation therapy, hormone therapy, surgery, cryosurgery, or a combination of therapies.[12] However, current therapies are less effective at treating metastatic cancers, and combined with the increased difficulty in detecting and treating metastatic cancer, most cancer deaths are due to metastatic disease instead of primary tumors.[10] Discovering ways to image these metastatic tumors, along with the primary ones, is hence the crucial step in combating cancer more effectively in our society.

3 Vitamin B_{12} (B_{12})

3.1 B_{12} Structure

B_{12}, also known as cobalamin, is one of the eight B vitamins.[14] Once described as "nature's most beautiful cofactor,"[15] B_{12} is a rare example of an organometallic compound in nature, and it is the only vitamin to possess a stable metal-carbon bond. In 1964, Dorothy Hodgkin won the Noble Prize in Chemistry for solving the crystal structure of the vitamin.[16]

Figure 3.1 shows the molecular structure of the vitamin.[1] B_{12} contains a six coordinate cobalt(III) atom that is encircled by a tetradentatecorrin ring, a 5,6-dimethylbenzimidazole with a phosphoribose unit termed the α-ligand, and a variable group termed the β-ligand positioned above the plane of the ring. This group can be a cyano, hydroxyl, methyl, or an adenosyl group.[17] B_{12} supplements are typically sold as cyanocobalamin, but this biologically inactive form can be converted into the biologically active forms that carry either a methyl group or a d'-deoxadenosyl group. Like all of the B vitamins, B_{12} is classified as highly water-soluble (10.2 mg/mL).[17]

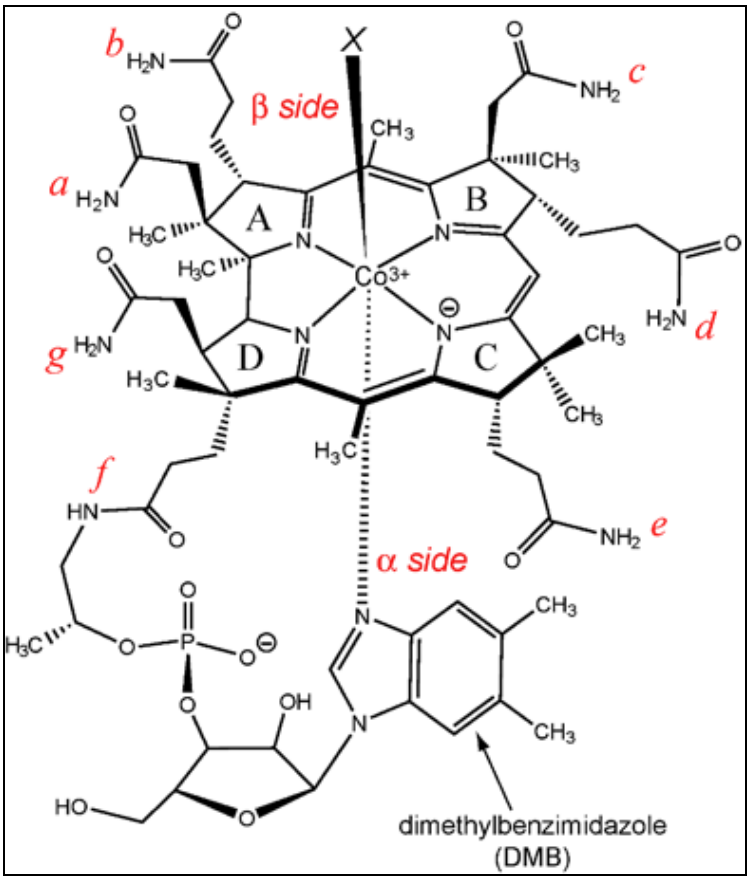

Figure 3.1. Structure of B_{12}, which includes a cobalt(III) bound to a variable group (R= cyano, methyl, adeosyl, or hydroxyl), a tetradentate corrin ring, and a 5,6-dimethylbenzamidazole phosphoribose moiety.

3.2 B_{12} Function

B_{12} serves as a cofactor for two distinct enzymatic processes.[18] In the cytoplasm, it is required by methionine synthase to convert homocysteine to methionine through a methylation reaction that is married to nucleotide synthesis.[18] Methionine is an essential amino acid. In the mitrochondrion, it is required by methylmalonyl-CoA mutase to convert L-methylmalonyl-CoA to succinyl-CoA in the metabolism of fatty acids.[18]

The devastating effects of B_{12} deficiencies demonstrate how essential the vitamin is to all cells in the body.[18] Moderate B_{12} deficiencies may occur as a result of limited dietary access or well as medical conditions that result in poor absorption and impaired transportation and metabolism of the vitamin,[19]and deficiencies commonly occur in individuals who do not consume animal products, in infants, and in the elderly.[20]

B_{12} deficiencies present with neurological symptoms, such as confusion, headaches, and depression, and with gastrointestinal symptoms, such as nausea, vomiting, and loss of appetite.[18]Additional symptoms include paleness, weakness, and fatigue.[18] Chronic or complete inability to uptake the vitamin leads to degeneration of nerve fibers, or pernicious anemia, which confers permanent neurological damage.[18]

3.3 B_{12} Uptake Pathway

Although mammalian cells require B_{12} for metabolism and growth, this essential cofactor must be obtained from external sources; therefore, mammals have evolved a selective uptake pathway that protects B_{12} from proteolytic degradation in the stomach and maximizes absorption and delivery of B_{12} to the cells that require it. This human B_{12} uptake pathway, shown as a scheme in Figure 3.2, includes three known transport proteins: intrinsic factor, transcobalamin, and haptocorrin.

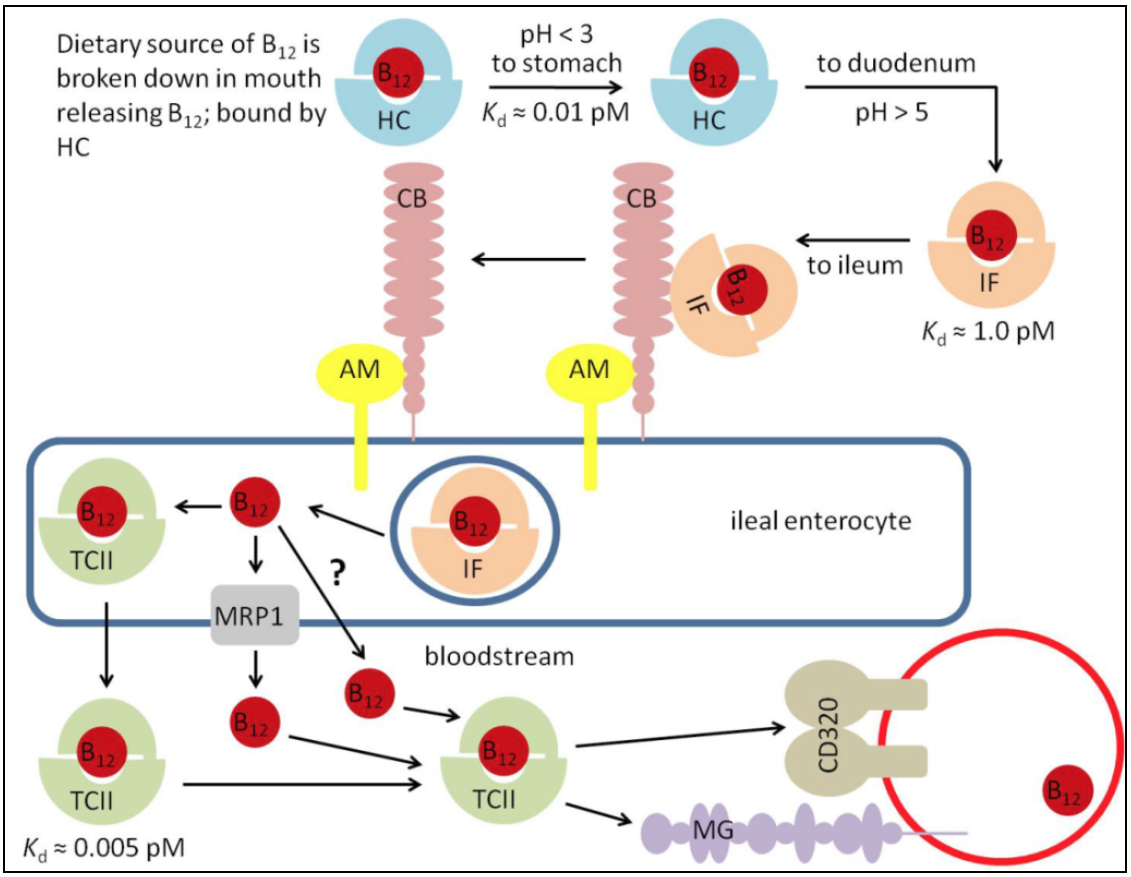

Figure 3.2. Dietary uptake pathway for B_{12}. Abbreviations used are defined as: (HC) haptocorrin; (IF) intrinsic factor; (CB) cubilin; (Am) amnionless; (MRP1) multi-drug resistance protein 1; (MG) megalin; (TCII) transcobalamin II; (CD320) transcobalamin II receptor.

3.3.1 Haptocorrrin (HC)

When a dietary source of B_{12} is ingested, it binds to HC, a heavily glycosylated protein, in the mouth.[18] In humans, HC is found in saliva, breast milk, and plasma.[18] HC remains bound to B_{12} and carries it through the upper gastrointestinal tract, protecting it from degradation via hydrolysis in the acidic environment of the stomach.[18]

3.3.2 Intrinsic Factor (IF)

When the HC-B_{12} exits the stomach and enters the duodenum, pancreatic enzymes degrade HC. The freed B_{12} binds to IF, a protein that is excreted by the gastric mucosa and the pancreas. Unlike HC, IF is not degraded by the pancreatic enzymes due to its heavy glycosylation.[18] The IF-B_{12} complex is transported through the intestine to the terminal ileum, where it is taken up into enterocyte cells by a complex composed of cubulin and amnionless known as the cubam receptor. This process is receptor-mediated endocytosis. In the ileal enterocyte, the cubilin-bound IF-B_{12} is broken down to give free B_{12}, which is released into the bloodstream through the basolateral side of the cell by the ABC transporter MRP1.[18]

IF is critical because it transports B_{12} to the ileal transport receptor, cubam; the cubam receptor does not bind free B_{12}, only the IF-B_{12} complex. Medical conditions such as autoimmune attack of the parietal cells or inborn errors of IF protein production demonstrate the importance of IF for B_{12} absorption, as these conditions result in a complete lack of B_{12} absorption and pernicious anemia.[18]

3.3.3 Transcobalamin (TCII)

Once in the plasma, free B_{12} binds to either TCII or HC, though the circulating TCII is responsible for transporting B_{12} to the cells of the body that require it. These cells take up the TCII-B_{12} through the transmembrane CD320

protein, a member of the LDL receptor family, which binds only B_{12}-bound TCII (holo-TCII). This receptor is present on the cell surface in virtually all tissues[21] and is expressed in proportion to the rate at which cells are proliferating.[22] Upon receptor-mediated endocytosis, the TCII-B_{12} is broken down in the acidic environment of the lysosome and free B_{12} is released into the cell for subsequent methylation or adenosylation and use in the cell.

3.4 Using B_{12} as a Probe for Cancer

Due to several inherent properties of both cancer cells (as reviewed above), the vitamin, B_{12} is ideal to use to target cancer cells for the delivery of imaging agents with minimum background uptake and harm to the host organism.

3.4.1 Increased TCII Receptors

Ideal cancer diagnostics therapeutics are those that selectively affect cancer cells but leave normal tissues unharmed; as such, it is important to identify and exploit characteristics of cancer cells that distinguish them from healthy cells. One such characteristic is the increased expression of vitamin receptors. In particular, it has been shown that the expression level of the receptor for the TCII, the CD320 receptor, is related to the rate at which the cell is growing and dividing.[22] Alberto et al. showed that rapidly growing and dividing cancer cells require excessive amounts B_{12}, and aggressive tumors have a high density of these CD320 receptors.[23] It is hypothesized that the increased expression of the CD320 receptor helps cells obtain B_{12} which is required for the biosynthesis of

nucleotides for increased cell proliferation.[18] This finding shows that the B_{12} pathway can be exploited to offer a tropism for cancer cells for the targeted delivery of imaging agents or therapeutics to rapidly growing tumors.

3.4.2 *De Novo* Expression of HC

Certain cancer cell lines express membrane-bound HC *de novo*.[1] Unlike the other transport proteins intrinsic factor and transcobalamin, HC binds B_{12} and B_{12} fragments.[18] The physiological role of HC is not yet fully known.[18] Waibel et al. analyzed HC expression in different tumor types and normal tissues, demonstrating strong HC positivity in seminoma of the testis, breast cancer, lung cancer, sarcoma, ovarian cancer, skin cancer, thyroid cancer, uterine cancer, and kidney cancer, among others.[1] By contrast, strong HC positivity of benign tissue was exclusively found in the liver. As a unique property of cancer cells, the *de novo* expression of HC in these specific tumors makes them attractive targets for B_{12} probes that would bind to the selectively expressed HC.[1]

3.4.3 Biocompatibility

B_{12} probes, which exploit the vitamin's supply route to target regions of extreme cell growth, are ideal due to high solubility in aqueous *in vitro* and *in vivo* conditions and a lack of toxicity dangers to the host.[17] There are no known cases of cytotoxicity associated with B_{12}.[1] In addition, because B_{12} is so essential, the uptake pathway is unlikely to be modified by mutation, suggesting that this vitamin-based probe would find long-term use in the field.[1]

3.4.4 Conjugation Sites on B_{12}

The B_{12} molecule offers several sites for conjugation chemistry, including the cobalt metal center, the 5,6-dimethylbenzimidazole phosphoribose unit, and the propionamide side chains.[1] The conjugation site was selected to minimize interference with B_{12}'s ability to bind with its transport proteins, ensuring that the probe would be recognized, transported, and internalized properly. Thus, instead of derivatizing the cobalt metal center or functionalizing the amides, conjugations were carried out at the 5' hydroxyl group of the phosphoribose moiety of B_{12}. This site was previously shown to be reactive in a coupling reaction with 1,1-dicarbonyl-di-(1,2,4-triazole) (CDT) coupling agent, and conjugates retained binding with IF and TCII.[24]

4 Fluorescence Imaging for *In Vitro* Imaging

4.1 Rhenium

The radioisotope of technetium, 99m-technicium (^{99m}Tc), has been described as the "medical isotope of choice for nuclear imaging."[25] Produced by the beta decay of ^{99}Mo in a commercial generator, ^{99m}Tc has a half-life of ~6 hours, which is long enough to be useful in diagnostic procedures but not so long as to be dangerous to the patient.[25] However, there is no stable isotope of technetium, so scientists use "cold" rhenium studies as a surrogate test that can then be translated to technetium for the development of a nuclear imaging diagnostic probe.

As congeners of group 7, technetium and rhenium have similar physical properties and coordination chemistry. While ^{186}Re(I) is not a commonly used fluorophore, is has a distinct excitation and emission profile, and the fluorescent ^{186}Re(I) can be used *in vitro* to test the efficacy of ligands for direct translation to radioactive ^{99m}Tc for use *in vivo*. Rhenium (and technetium) *fac*-tricarbonyl bearing polypyridyl ligands have been developed and studied for use in the field of cellular imaging.[25,26,27]

4.2 Utility of a B_{12}-based Fluorescent Probe

A fluorescent B_{12}-based probe would find use in a number of research settings. In the Doyle lab, such a construct could be used to investigate the association and internalization of B_{12} based therapeutics and imaging agents in a

cellular system prior to *in vivo* models. Positive uptake would suggest that specific chemical modifications to B_{12} did not critically interfere with transport protein binding and recognition and that the B_{12} conjugate was recognized and internalized by living cells. In research groups around the world, a fluorescent B_{12}-based probe would allow for the preliminary screening of cultured cell lines to confirm the presence of certain receptors that are important in the B_{12} uptake pathway, such as cubilin. Finally, for laboratories that are studying the differential expression of these receptors in varied tissue samples, such a probe would provide a confirmation of the receptor on the cellular level—functionality that cannot be obtained from biochemical methods such as reverse transcriptase polymerase chain reaction (RT-PCR) or Western blot.

4.2.1 Previous B_{12}-based Fluorescent Probe Constructs

The first generation fluorescent B_{12}-basedprobe for use *in vitro* studied in the Doyle lab was designed to target cubilin expressed in cancerous cells. This probe, B_{12}-BQBA-[$Re(CO)_3$], incorporated a ligand *N,N*-bis(quinolinoyl) (BQBA) to chelate the Re(I).[26] Doyle et al. synthesized, purified, and characterized the probe, and then screened placental choriocarcinoma BeWo cells to show uptake of B_{12}-BQBA-[$Re(CO)_3$] via an IF-cubilin receptor mediated endocytosis mechanism.[26] This work was published in 2009 in the Journal of Medicinal Chemistry.

4.3 B_{12}-[$Re(CO)_3$]-Thiazole

The utility of the first generation B_{12}-BQBA-[$Re(CO)_3$] probe was severely limited by its poor solubility in aqueous solvents, and the second generation probe was designed to be more water-soluble and thus more useful in a water-based cell system.[27] Instead of the BQBA, a bifunctionalthiazole ligand that was first described by the Valliant group was chosen based on its ability to both chelate the Re(I) and offer an amino group for coupling with B_{12}.[27] This ligand was also expected to be more polar, and thus, more water-soluble. The final compound, a water-soluble B_{12}-Re(I) probe incorporating the thiazole linker-chelator moiety, was used to demonstrate the presence of cubilin in A549 lung cancer cells. The entire synthetic scheme is shown in Figure 4.1.

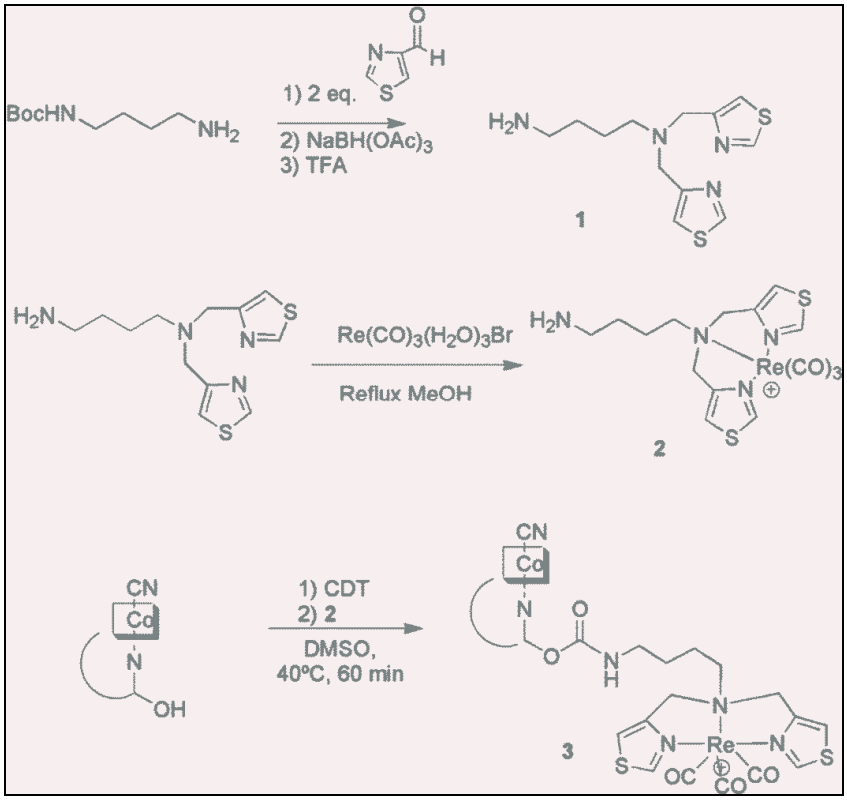

Figure 4.1. Synthesis of B_{12}-[$Re(CO)_3$]-Thiazole.

4.3.1 Synthesis, Purification, and Characterization of 1,1, bisthiazole (1,4) di-aminobutane

1,1, bisthiazole (1,4) di-aminobutane (**1**) was synthesized by combining N-Boc-1,4-butanediamine (100 mg, 0.53 mmol) and thiazole-4-carboxaldehyde (120 mg, 1.06 mmol) in 5 mL of anhydrous dichloroethane and stirred under $N_{2(g)}$ at room temperature. After 30 minutes, sodium triacetoxyborohydride (225 mg, 1.5 mmol) was added and the reaction was stirred for an additional 16 hr. The solvent was removed *in vacuo,* and the reaction was redissolved in 10% MeOH/10% TFA in H_2O and stirred for 3 hr.

1 was purified by RP-HPLC using an analytical C_{18} column (Agilent Eclipse XDB-C18 9.4 mm X 250 mm, 3 µm particle size) on an Agilent 1100 series instrument with a quaternary pump and UV detection at 254 nm. The solvents for purification included (A) 0.1% TFA/water and (B) 0.1% TFA/MeCN, and the flow rate was 1 mL/min. The method was a gradient of 0-20% B over 5 min, followed by an increase to 40% B over another 4 min. Under these conditions, **1** eluted with a T_r of 3.4 min. The yield of **1** was 60%.

Purity of **1** was confirmed via ^{1}H NMR and MALDI-ToF/MS. An ^{1}H NMR spectra, taken in deuterium oxide (D_2O) at 300 MHz, confirmed the proposed structure of **1**, showing ^{1}H NMR peaks (in δ): 9.06 s, 2H; 7.83 s, 2H; 4.57 m, 4H; 3.24 t, 2H; 3.00 t, 2H; 1.92 m, 2H; 1.67 m, 2H. MALDI-ToF/MS

showed a peak consistent with **1** at 283.15 *m/z*, the expected $M[H]^+$ value of 283.1 amu.

4.3.2 Synthesis, Purification, and Characterization of $Re(CO)_3$-1,1, bisthiazole (1,4) di-aminobutane complex

The purified ligand **1** was labeled with rhenium to give $Re(CO)_3$-1,1, bisthiazole (1,4) di-aminobutane complex (**2**). **1** (20 mg, 0.07 mmol) and $Re(H2O)_3(CO)_3Br$ (3 mg, 0.07 mmol) were dissolved in MeOH and refluxed for 3 h. The solvent was removed *in vacuo* and the residue was redissolved in 10% MeOH in H_2O.

2 was purified by RP-HPLC using an analytical C_{18} column (Agilent Eclipse XDB-C18 9.4 mm X 250 mm, 3 µm particle size) on an Agilent 1100 series instrument with a quaternary pump and UV detection at 254 nm. The solvents for purification were (A) 0.1% TFA/water and (B) 0.1%TFA/MeCN, and the flow rate was 1 mL/min. The method was a gradient of 0-20% B over 5 minutes, followed by an increase to 40% B over another 4 minutes. Under these conditions, **2** eluted with a T_r of 5.2 min. The yield of **2** was 73%.

Purity of **2** was confirmed via ^1H NMR and MALDI-ToF/MS. An ^1H NMR spectrum taken in deuterium oxide (D_2O) at 300 MHz, confirmed the proposed structure of **2**, showing ^1H NMR peaks (in δ): 9.57 s, 2H; 7.67 s, 2H; 4.67 m, 4H; 3.8 t, 2H; 2.90 t, 2H; 1.94 m, 2H; 1.70 m, 2H. MALDI-ToF/MS

showed a peak consistent with **2** at 553.05 *m/z*, the expected $M[H]^+$ of 553.04 amu.

4.3.3 Synthesis of B_{12}-[$Re(CO)_3$]-Thiazole (2)

2 was coupled to the 5' hydroxyl of the ribose group of B_{12} via 1,1'-carboyl-di-(1,2,4-triazole) (CDT) coupling to give B_{12}-[$Re(CO)_3$]-Thiazole(**3**). B_{12} (10 mg, 0.006 mmol) and CDT (2 mg, 0.010 mmol) were dissolved in dry DMSO and heated to 40°C for 1 hr under $N_{2(g)}$ to activate the hydroxyl group for coupling with an amino group. **2** (4 mg, 0.007 mmol) was added to the reaction and the reaction was left stirring under $N_{2(g)}$ overnight (Figure 4.2). After 16 hr, the reaction was precipitated using acetone and diethyl ether to give a deep red precipitate that was redissolved in 10% MeOH in H_2O.

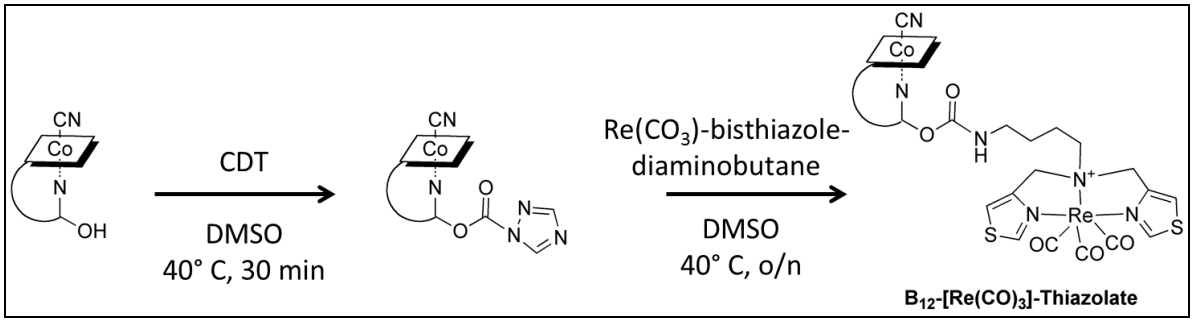

Figure 4.2. CDT-Coupling of 2 to B_{12}.

3 was purified by RP-HPLC using an analytical C_{18} column (Agilent Eclipse XDB-C18 9.4 mm X 250 mm, 3 µm particle size) on an Agilent 1100 series instrument with a quaternary pump and UV detection at 254 nm. The solvents for purification included (A) 0.1% TFA/water and (B) 0.1%TFA/MeCN, and the flow rate was 1 mL/min. The method was a gradient of 0-20% B over 5

minutes, followed by an increase to 40% B over another 4 minutes. Under these conditions, **3** eluted with a T_r of 7.3 min (Figure 4.3). The yield of **3** was 13%.

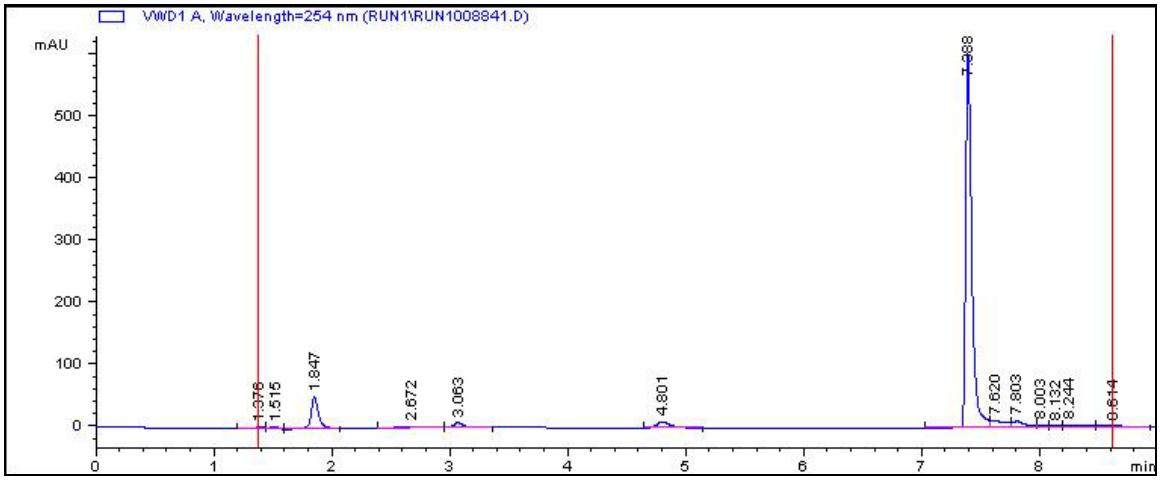

Figure 4.3. RP-HPLC trace. 3 elutes at 7.3 minutes.

Purity of **3** was confirmed via ^{1}H NMR and MALDI-ToF/MS. An ^{1}H NMR spectrum, taken in deuterium oxide (D_2O) at 300 MHz, confirmed the proposed structure of **3**, showing ^{1}H NMR peaks (in δ): 9.19 d, 2H; 7.74 s, 2H; 7.24 s, 1H, 7.04 s, 1H; 6.48 s, 1H; 6.26 s, 1H, 6.02 s, 1H. MALDI-ToF/MS showed a peak consistent with **3** at 1907.24 *m/z*, the expected M^+[-CO] of 1907 (Figure 4.4 and 4.5).

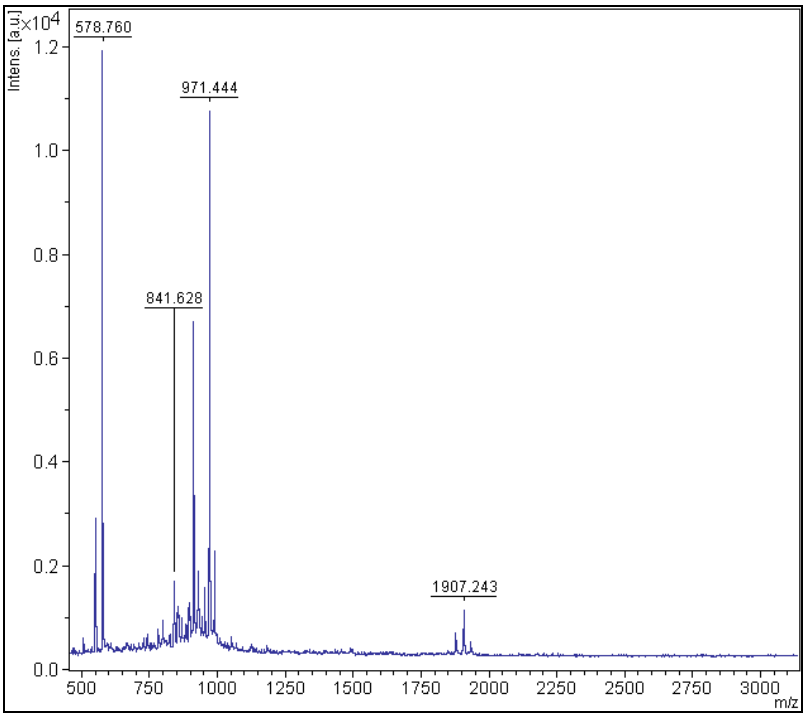

Figure 4.4.MALDI-ToF/MS of 3, showing expected mass at 1907 amu for the M[H]$^+$.

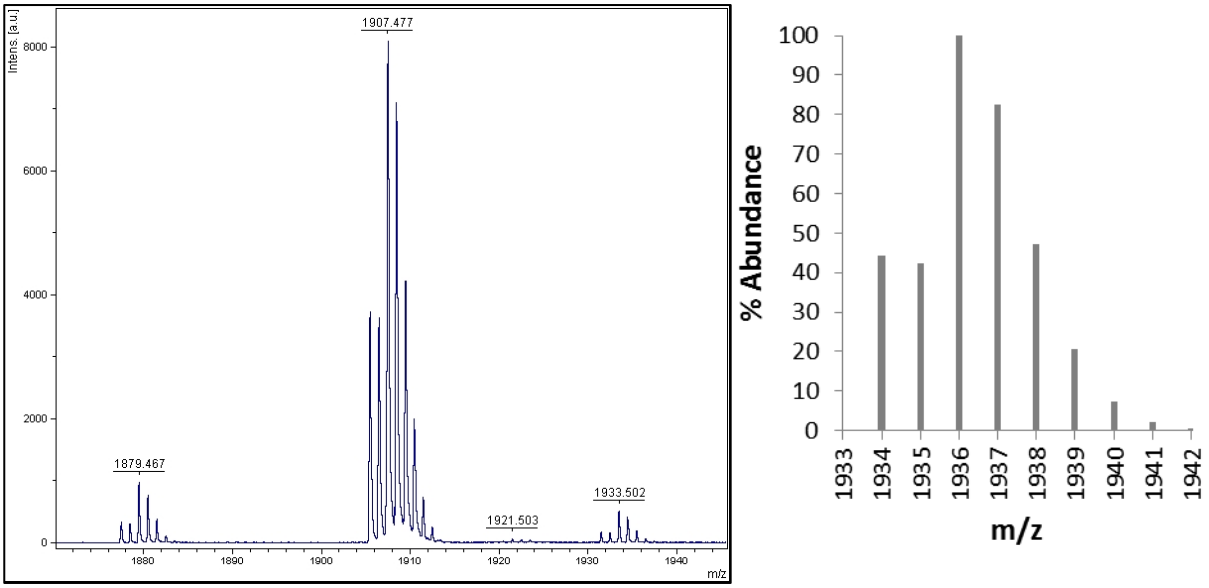

Figure 4.5. The calculated (left) and experimental (right) isotopic patterns of 3, without one CO group, are equivalent and consistent with M[H]$^+$.

4.4 Fluorescent Studies of 3

Fluorescence spectroscopy was carried out on a Horiba JobinYvon (Kyoto, Japan) FluoroMax-4 spectrofluorometer in PBS buffer. **3** had an absorption maximum of 466 nm (Figure 4.6). The fluorescence emission spectrums of **3** were measured with excitation at 458 nm (Figure 4.7) and 488 nm (Figure 4.8).

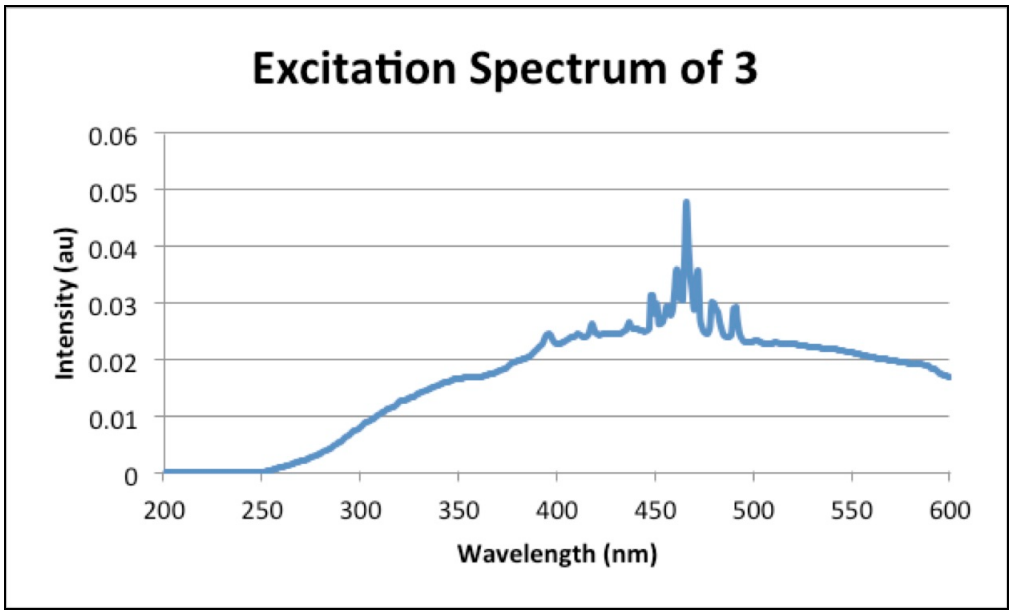

Figure 4.6. Excitation wavelength scan (200-600 nm) for 3.

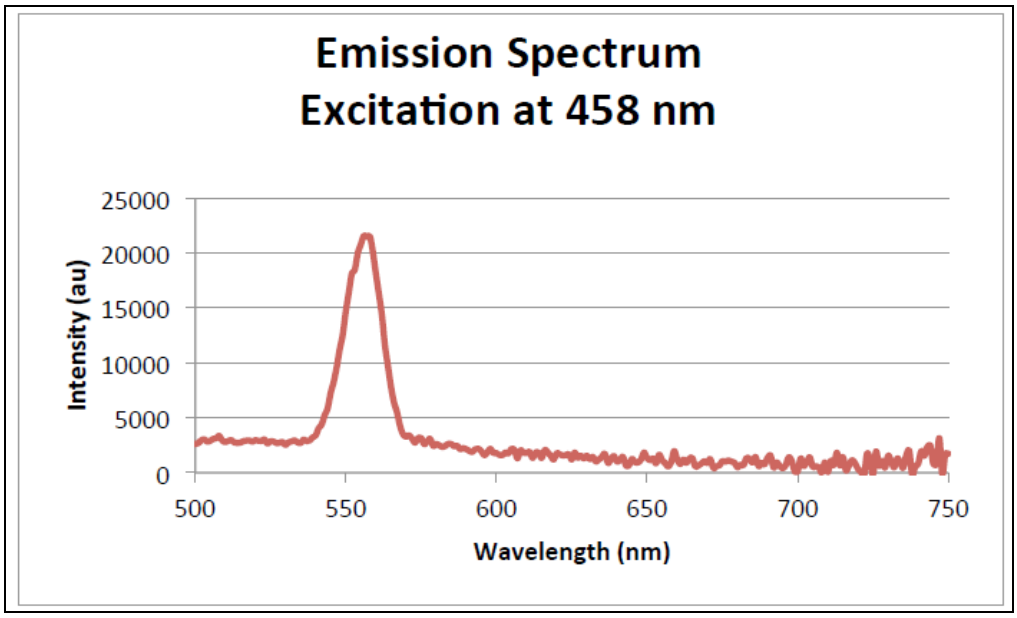

Figure 4.7. Emission spectrum of 3 upon excitation at 458 nm.

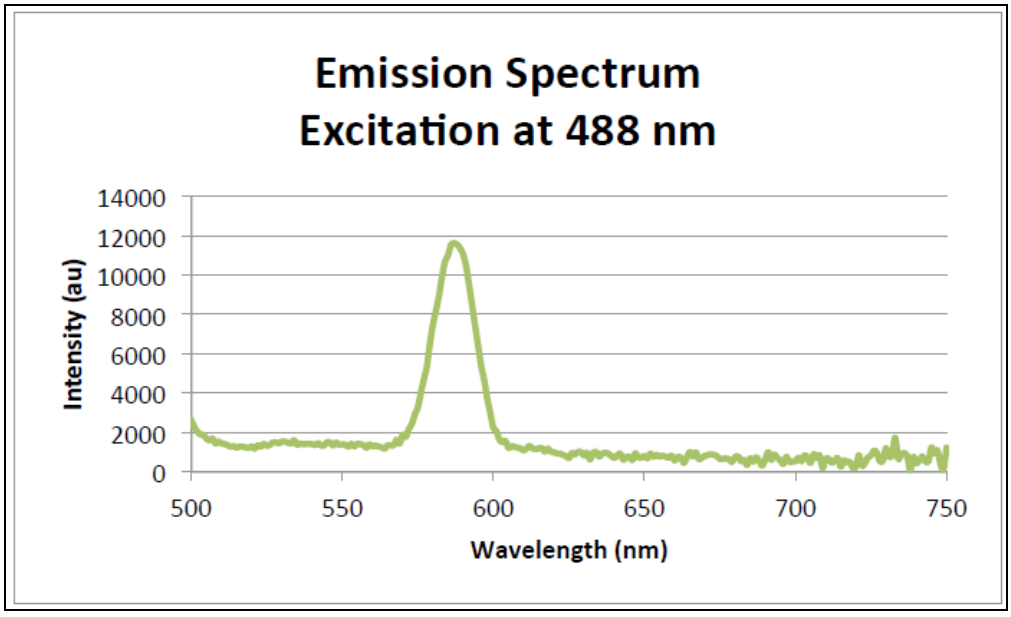

Figure 4.8. Emission spectrum of 3 upon excitation at 488 nm.

Compared to the unconjugated rhenium-labeled fluorescent tag **2,** the full probe **3** showed weaker fluorescence intensity. The likely cause for the decrease in fluorescence upon conjugation with B_{12} is quenching by the B_{12} molecule.[28]

When IF was added, the fluorescence improved significantly in terms of intensity and emission maximum, suggesting that IF binding to **3** relieves the quenching effect. Upon IF addition, a 15-fold increase in fluorescence intensity was observed, and the emission maximum blueshifted ~30 nm from ~555 to ~525 nm.

The quenching nature of B_{12} was further confirmed by adding excess B_{12} to IF-**3.** A decrease in fluorescence was observed when a 100-fold excess of pure B_{12} was added to IF-**3**, as the excess B_{12} resulted in a loss of binding of IF to **3.** Figure 4.9 shows the fluorescent emission spectrum of **3**, IF-3, and IF-**3** with 100x excess of free B_{12}. When bovine serum albumin (BSA) was added as a control, the fluorescence intensity increased only 5% and the emission maximum did not shift (Figure 4.10).

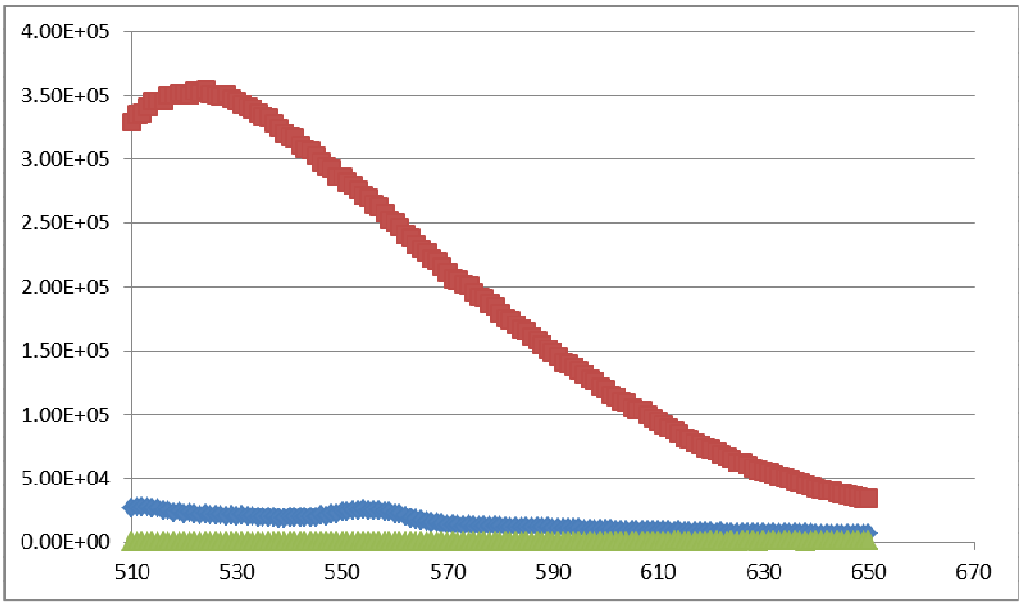

Figure 4.9. Fluorescent emission spectrum of 3 (blue), IF-3 (red), and IF-3 with 100-fold excess of free B_{12}(green), demonstrating a quenching effect by excess B_{12}.

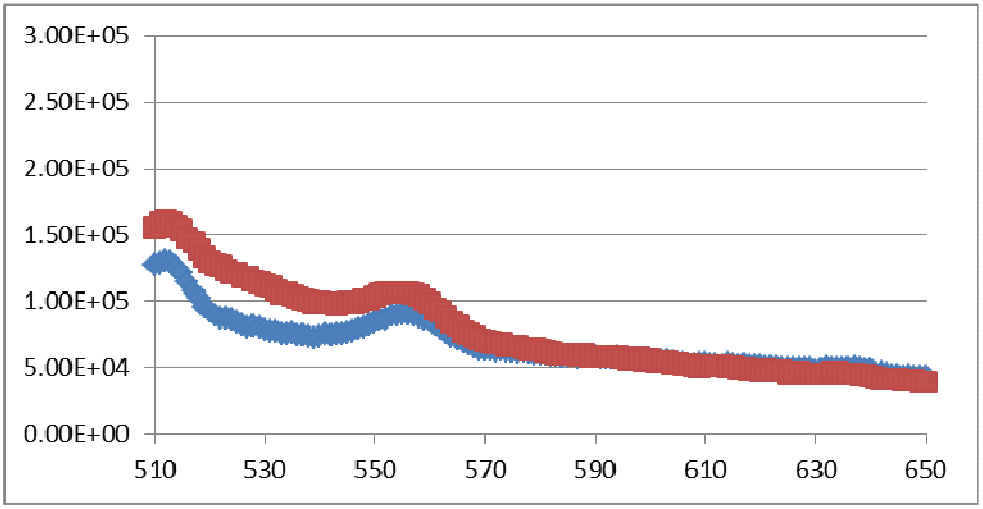

Figure 4.10. Fluorescent emission spectrum of 3 (blue) and bovine serum albumin (BSA)/3 (red). Unlike IF, the addition of BSA did not alter the emission maxima, suggesting that 3 can be used to follow IF binding in a facile manner.

The quenching issue observed for free **3** is not a concern for *in vitro* or *in vivo* experiments because **3** must be bound to IF in order to be recognized and internalized by the cubilin receptor; IF binding relieves the quenching and maximizes the fluorescent signal. However, the dramatic effects of IF binding on the photophysical properties of **3** could be exploited to monitor binding of IF to **3** in other studies.

4.5 Screening of A549 Lung Cancer Cells with IF-3

After fluorescence studies, IF-**3** was added to A549 lung cancer cells and studied via confocal microscope to look for uptake of IF-**3**.

4.5.1 Cell lines and culture conditions

The A549 lung cancer cell line (ATCC CCL-185) was cultured in Millipore 250 mL culture bottles with vented lids and incubated in a VWR mammalian incubator at 5% CO_2 and 95% humidity, conditions meant to mimic physiological conditions. Cells were grown in F-12K media supplemented with penicillin (10 000 U), 10 mg mL^{-1} streptomycin, and 10% fetal bovine serum (FBS). Prior to testing, cells were passed in this F12K media and penicillin–streptomycin solution.

For confocal experiments, 200,000 cells were plated onto MatTek 35 mm glass bottom culture dishes and incubated overnight. The media was then replaced with phosphate-buffered saline (PBS) containing 100 µmol of IF-**3** and incubated

for 1 hour. After incubation, the cells were washed with PBS to remove any excess and unbound IF-**3**.

4.5.2 Confocal Microscopy

Cells were viewed under a Zeiss LSM 710 Pascal confocal microscope with Zen 2009 image analysis software equipped with argon ion and HeNe lasers. Fluorescence was observed with a 63X objective with an excitation at 458 nm and 488 nm lasers. The laser power was set to 20% 458 nm and 35% 488 nm. The signal was detected using a 493–630 nm filter, with the master gain set to 281 and the digital game set to 9.86 with a pinhole of 49 μm.

Initially, when the cells excitation was carried out by either a 458 nm laser or a 488 nm laser, the confocal microscopy conditions needed to detect the weak fluorescent signal of IF-**3** also produced natural cellular fluorescence in A549 control cells. This background autofluorescence is thought to be from molecules naturally present in the cell, such as flavins, porphyrins, and other aromatic compounds.[29] Because it was difficult to distinguish the autofluoresence from the fluorescent signal of IF-**3**, excitation was attempted at both 458 nm and 488 nm simultaneously. This dual-excitation produced a maximized signal, kept both pinhole and detector gain low, and did not produce background fluorescence in the control cells. The control cells are shown in Figure 4.11. These conditions successful eliminated the potential for a false positive result.

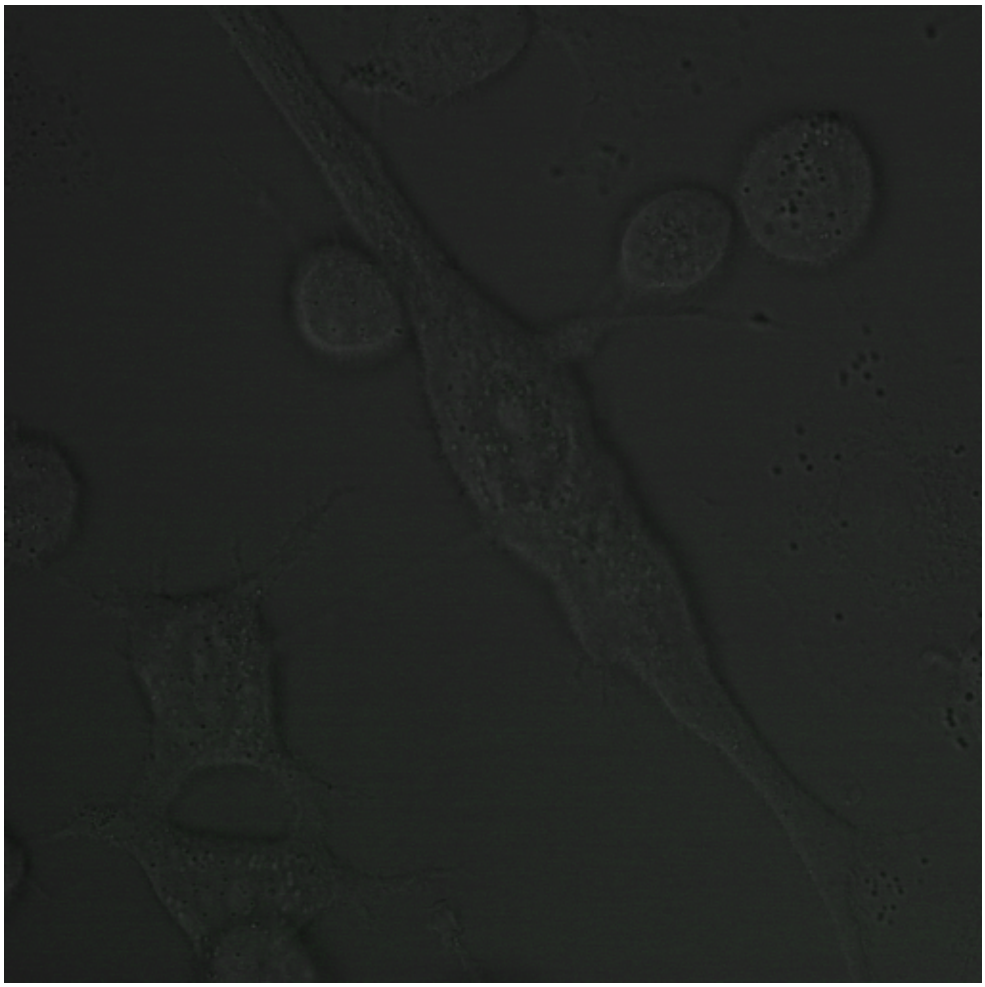

Figure 4.11. 63X magnification of A549 cell controls (i.e. no addition of IF-3) under matching confocal microscope test conditions.

Under these conditions, it was shown that the IF-**3** was internalized in A549 cells with clear cytoplasmic localization (Figure 4.12). No localization in the nucleus was observed.

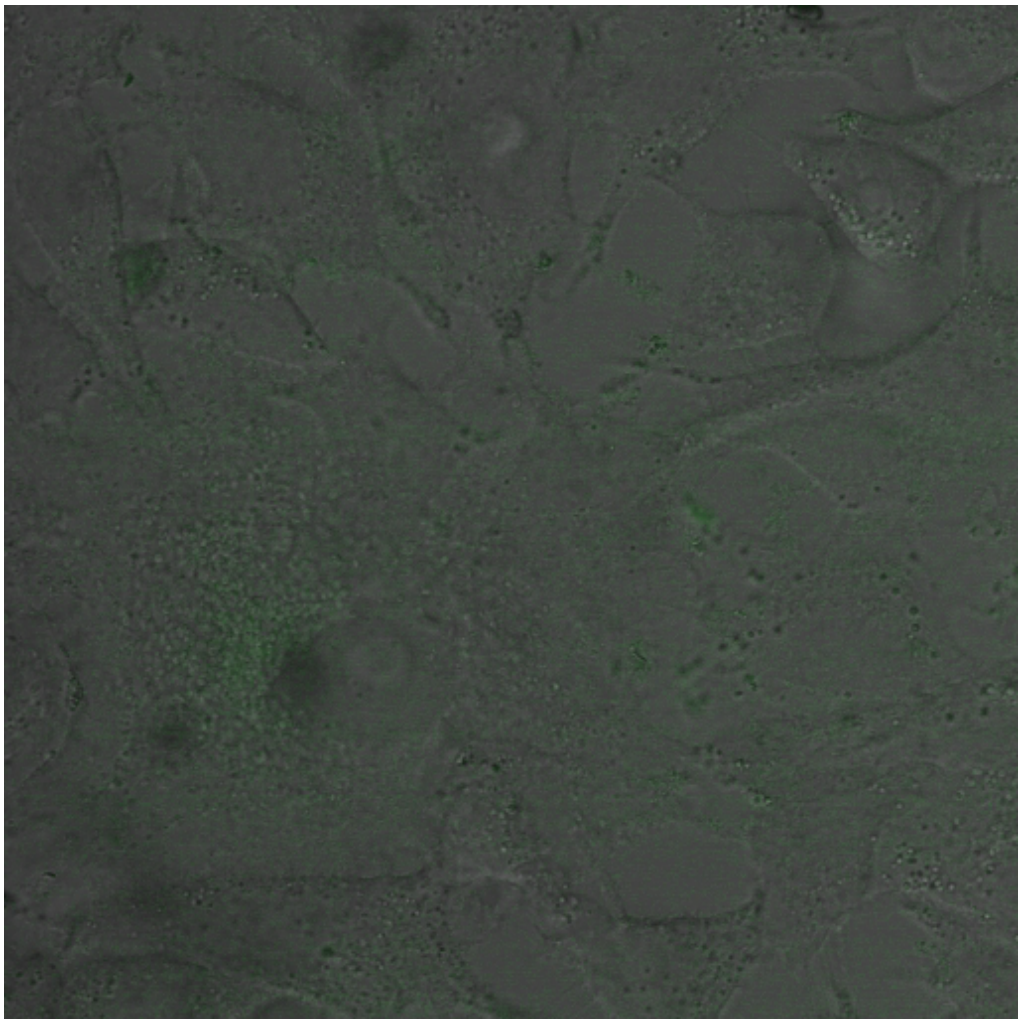

Figure 4.12. 63x magnification image of uptake of IF-3 in A549 cancer cell line with dual excitation at 458 and 488 nm at room temperature (compare to Figure 4.11 control). IF-3 is localized in the cytoplasm.

In order to confirm that the IF-**3** was targeting the cubilin receptor and that the observed uptake was due to receptor-mediated endocytosis, the experiment was repeated at 4 °C. At 4 °C, uptake due to receptor mediated endocytosis would be halted, while uptake due to passive diffusion would not be affected. The cells were pre-chilled for 30 minutes, after which time a chilled solution of

IF-**3** was added. The cells were incubated at 4 °C for 1 hr and visualized via confocal microscopy under the same conditions. The cells showed no internalization of the IF-**3**, but cell surface binding was still observed—an expected result, as receptor recognition is not lost at low temperature (Figure 4.13).

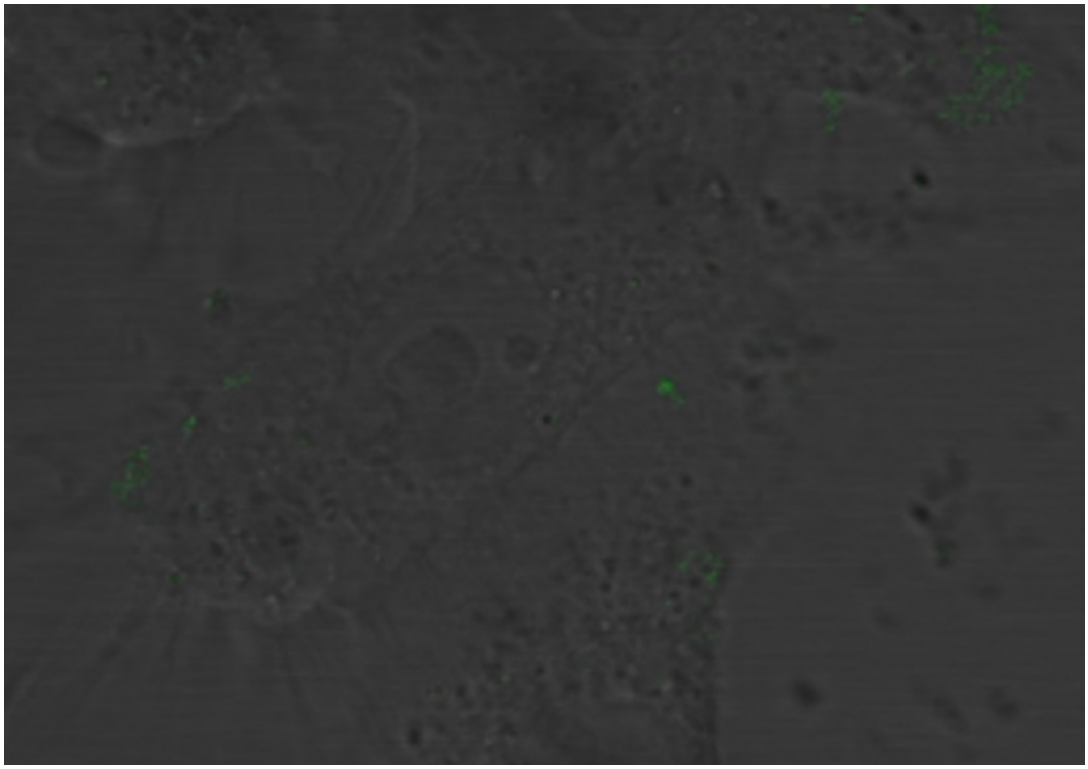

Figure 4.13. 63x magnification image showing uptake studies of IF-3 in A549 cells performed at 4 °C. No internalization was observed.

Based on the quenching effect of free B_{12}, a B_{12} challenge experiment was determined to be of limited utility. Excess B_{12} was expected to quench the fluorescence of IF-**3**, thereby potentially yielding a false negative which would be difficult to distinguish from blocked uptake.

4.6 RT-PCR and Western Blot Analyses

Expression of cubilin was independently confirmed by reverse transcriptase polymerase chain reaction (RT-PCR) and western blotting through collaboration with the University of Aarhus in Denmark.

4.6.1 RT-PCR

RT-PCR was carried out to confirm the expression of cubilin on the level of mRNA. RNA from A549 cells was extracted using QiagenRNeasy mini kit as per manufacturer's instructions (Qiagen). The 'One step RT-PCR kit' (Qiagen) was used. Total PCR reaction volumes were 25 mL and reaction included: 200 ng of RNA template, 5x Buffer [Tris.Cl, KCl, $(NH_4)_2SO_4$, 12.5 mM $MgCl_2$, DTT; pH 8.7], 1xQ solution, 0.4 mM of each deoxynucleotide triphosphate (dNTP), 15 pmol of each primer, 1.0 μL enzyme mix (Omniscript and Sensiscript Reverse Transcriptases, HotStartTaq DNA polymerase). Non-template controls were performed for each set of primers and template. The reverse transcription and amplification were carried out under the following incubation program: 30 min at 50 °C, 15 min at 95 °C, 35 cycles at 94 °C for 1 min, 50 °C for 1 min, 72 °C for 3 min, and finally 10 min at 72°C. Amplification products (20 μL) were analyzed on a 2% agarose gel and visualized using SybrGreen. The sizes of the separated bands were estimated by comparison with a 100 bp DNA marker. Cubilin mRNA was detected in A549 cells by RT-PCR.

4.6.2 Western Blot

A western blot was carried out to confirm the expression of cubilin on the protein level. A549 cells were lysed on ice in PBS buffer (10 mm NaH_2PO_4, 150 mm NaCl, 6 mm $CaCl_2$) including 1% Triton X-100 (Merck) and complete mini EDTA-free protease inhibitor cocktail tablets (Roche Diagnostics), pH 7.4. Protein samples were then boiled in sample buffer (20 mm Tris, pH 6.8, 5% SDS, 17.4% glycerol and pyronin Y) and separated by sodium dodecyl sulpate-polyacrylamide gel electrophoresis (SDS-PAGE) using 3-8% acrylamide gels. After the gel electrophoresis, proteins were blotted onto a polyvinylidenedifluoride membrane. Immunoblotting was performed using anti-cubilin antibody (at 2 μg/ml) as primary antibody and alkaline phosphatase-conjugated anti-rabbit (1:50,000). Proteins were visualized using 5-bromo-4-chloro-3-indolyl-phosphate-nitro blue tetrazolium.

Cubilin protein was detected by western blot, although the level of expression was low overall, compared to the previously characterized cubilin expression in the Brown Norway rat yolk sac cell line BN16. The cubilin protein detected in A549 cells was compared with purified cubilin control protein purified by IF-B_{12}-affinity chromatography from human kidney. The protein from A549 cells appeared to be full length and of the same size as the kidney control protein. The Western blot is shown in Figure 4.14.

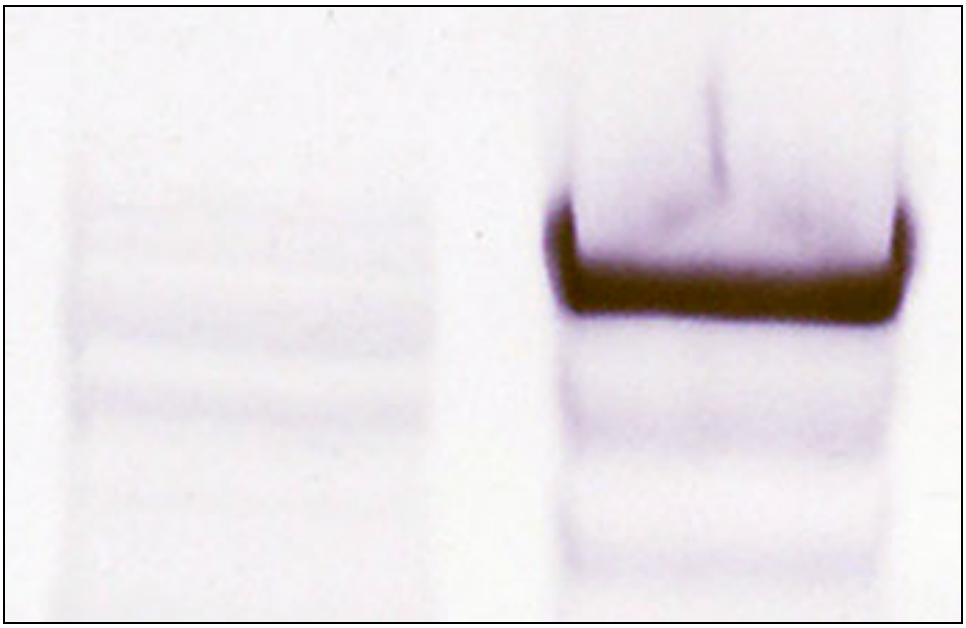

Figure 4.14. Western blot analysis of lysate of A549 cells. Lane 1: lysate of A549 cells. Lane 2: control cubilin protein purified from human kidney by IF-B_{12} affinity chromatography.

This work was published in *Chemical Communications* in 2011 in a paper titled "A water soluble vitamin B_{12}-Re(I) fluorescent conjugate for cell uptake screens: use in the conformation of cubilin in the lung cancer line A549.[v] *Chemical Communications* is the premier journal of the Royal Society of Chemistry.

4.7 Future work: Translation of *in vitro* Probes for *in vivo* use with Re(I) to ^{99m}Tc

The Re(I) -B_{12} probe can be readily translated to *in vivo* studies with minimal modifications to the overall ligand and conjugation process. The Re(I) coordinated to the thiazole ligand can be readily switched to a radioactive

derivative containing ^{99m}Tc and studied using single photon emission computer tomography (SPECT) scanning.[30] With ideal nuclear properties for clinical application and commercial availability, ^{99m}Tc is used in most diagnostic procedures today, and this system could be used as a targeted therapeutic in nuclear medicine.[25]

The functional role cubilin in lung cancer cells is unknown, and the finding of cubilin in these cells warrants further investigation. Looking forward into the development of therapeutics, these results on the presence of cubilin in lung cells also suggests the possibility of targeting drugs in lung cancer cells *in vivo* by aerosolizing B_{12}-drug conjugates—a substantial advance in cancer treatment.

5 Positron-Emission Topography *In Vivo* Imaging

5.1 PET Scanning

Within nuclear medicine, there exist two main non-invasive imaging techniques: single photon emission computer tomography (SPECT) and positron-emission tomography (PET) scanning.[25] Of the two, PET scanning provides higher resolution and sensitivity.[25] PET uses a radioactive element, such as fluorine-18, oxygen-15, carbon-11, or nitrogen-13, which decays through the emission of a positron that collides with an electron to produce gamma rays. These gamma rays are detected and compiled by a PET scanner and used to reconstruct a computerized image of the body. Clinically, the most commonly used radioactive imaging agent is fluorine-18 tagged to fluorodeoxyglucose (FDG), and the use of PET technique has grown since the late 1990s, when the FDA approved FDG and PET scanners were made mobile.[31]

As a diagnostic tool, PET scanning is valuable because it can be adjusted to detect and monitor a variety of physiological processes in various organs and parts of the body.[32] The increased sensitivity of PET scanning allows for the use of doses of radiolabelled imaging agents that are too small to cause pharmacological effects.[32]

5.2 Copper-64

In the growing field of molecular imaging, research has focused on developing, screening, and testing radiolabelled target agents for clinical use. In

particular, attention has been focused on PET imaging agents incorporating copper-64, (^{64}Cu), a radioactive isotope of copper.[32] ^{64}Cu has a half-life of 12.7 hours, which is long enough to allow for regional distribution but is not so long that the patient is at risk for prolonged radiation exposure.[32] In addition, it is readily synthesized on a cyclotron and a number of different ligands can be adapted for its use.[32]

However, copper is an important metal physiologically, and copper homeostasis is tightly regulated by both intracellular and extracellular copper-binding molecules. Therefore, it is essential that any radiolabeled copper species does not disturb other copper-dependent processes in the body. A viable copper chelate for biological use must be both thermodynamically stable and kinetically inert to prevent the release of the copper metal.[33]

Many of the current radiopharmaceuticals incorporating copper radioisotopes are bifunctional chelators that provide both a site for stable copper labeling and also chemical groups to covalently attach to biologically active molecules.[34] The chelators most commonly utilized for labeling copper radionuclides to biomolecules are analogues of 1,4,8,11-tetraazacyclotetradecane-1,4,8,11-tetraacetic acid (TETA).[34] However, these "non-bridged" macrocyclic ligands show limited *in vivo* stability.[34] Recent literature reports a higher degree of kinetic stability using bicyclic tetraazamacrocycles, the ethylene "cross-

bridged" cyclam (CB-cyclam) derivatives,[34] which showed no decomposition and rapid clearance from all tissues.[34]

5.3 B_{12}-ethylenediamine-1,4,7,10-tetraazacyclododecane-N',N'',N''',N''''-tetraacetic acid (B_{12}enDOTA)

Because these copper radionuclides covalently attached to biological molecules hold such great promise for diagnostic imaging and targeted radiotherapy, a B_{12}-based probe was constructed by conjugating B_{12} with a linker molecule, ethylenediamine (en), and a metal-chelating macrocyclic ligand, 1,4,7,10-tetraazacyclododecane-N',N'',N''',N''''-tetraacetic acid (DOTA). The resulting compound, B_{12}enDOTA (**1**), offers a site for the labeling to produce a radio labeled probe. **1** was purified by a two-step method involving an analytical anion exchange column and a C18 analytical column on reverse phase HPLC (RP-HPLC). The purity of **1** was confirmed by nuclear magnetic resonance spectrometry (^{1}H NMR) and matrix-assisted laser desorption/ionization-time of flight mass spectrometry (MALDI-TOF MS). In collaboration with the Washington University Medical School in St. Louis, Missouri, **1** was labeled with ^{64}Cu. Given the strong success of my initial ^{64}Cu-labeling experiments—showing 100% radiolabeling—the labeled analogue of **1** was tested *in vivo* in a mouse model.

5.3.1 Synthesis of 1

The first step of the synthesis was to functionalize the 5'hydroxyl group on the ribose moiety of B_{12} to an amine group for future peptide coupling reactions with the macrocyclic ligand. B_{12} (cyanocobalamin, 100.0 mg, 73.8 mmol) was activated with 1.45 equivalents of 1,1'-carboyl-di-(1,2,4-triazole) (CDT) (17.6 mg, 107.3 mmol) in 6 mL dry dimethyl sulfoxide (DMSO) at 40 °C for 1 hr under $N_{2\,(g)}$. Ethylenediamine (en) (4.59 μL, 68.7 mmol) and triethylamine (TEA) (9.59 μL, 68.8 mmol) were diluted in 1 mL dry DMSO. The CDT-activated B_{12} was added drop-wise over 30 min to the en solution. The reaction solution was stirred under $N_{2\,(g)}$ for 3 hr at 40 °C. After 3 hr, the reaction product was crashed out of DMSO using 4:1 diethyl ether/acetone solution, spun down at 4000 rpm for 10 min, and dried *in vacuo* overnight.

In the second synthesis reaction, the carboxylic acid arm of the macrocyclic ligand (DOTA) was conjugated to the free amino group of the B_{12}en conjugate via peptide coupling to give **1**. Because DOTA offers reactive four carboxylic acid arms, the DOTA was added in two equivalents excess to encourage the formation of a 1:1 B_{12}en:DOTA conjugate, assuming a yield of 100% for the B_{12}-ethylenediamine (B_{12}en) reaction, (106 mg, 73.8 mmol).

DOTA was activated using the water soluble 3-(ethyliminomethyleneamino)-N,N-dimethyl-propan-1-amine (EDC) coupling agent with *N*-hydroxysulfosuccinimide (sulfo-NHS) to increase coupling

efficiency. Two equivalents of DOTA (59.4 mg, 0.147 mmol) and 2.5 equivalents of sulfo-NHS (47.9 mg, 0.221 mmol) were dissolved in 1 mL 100 μM sodium phosphate (pH 6.5). EDC (30.9 mg, 0.162 mmol) was dissolved separately in 50 μL of the same buffer and added drop-wise over 20 min to the DOTA and sulfo-NHS solution. After the solution was allowed to activate at room temperature for 30 min, B_{12}en was dissolved in 2 mL 100 μM sodium phosphate (pH 6.5) and was added to the activated DOTA. The reaction was left stirring overnight at room temperature. Figure 5.1 shows the entire synthesis of **1**.

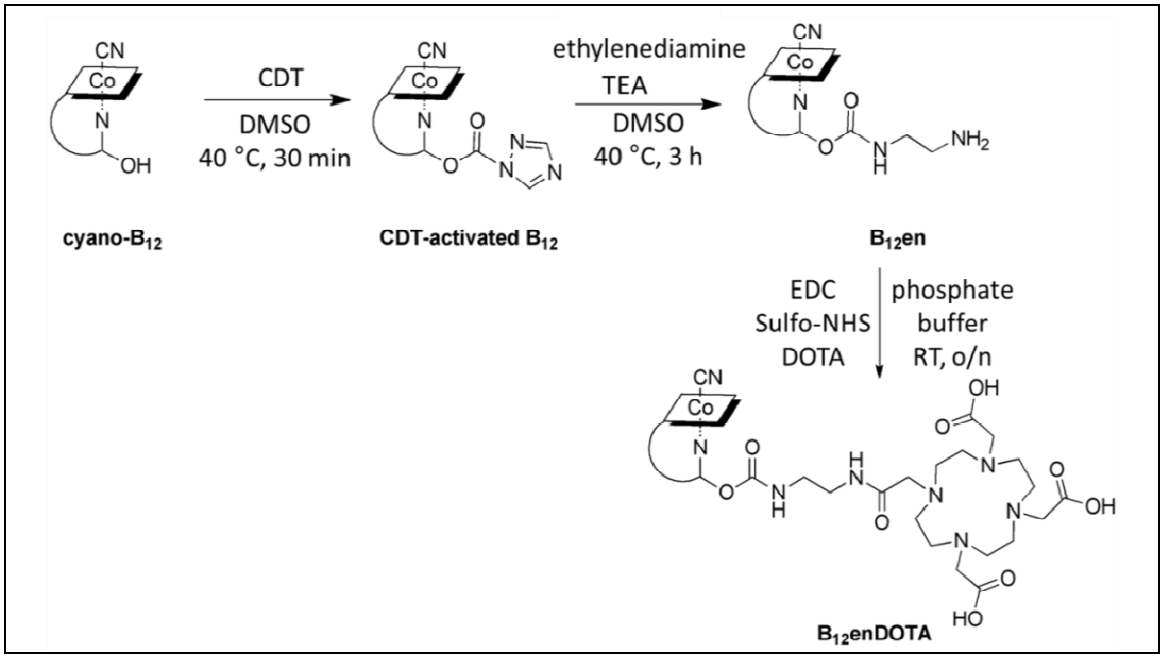

Figure 5.1: Schematic of the Synthesis of 1

5.3.2 Purification of 1

A two-step purification scheme was to first separate **1** from unreacted B_{12} and B_{12}en, and second from other oligomers that formed. Both purifications were performed on RP-HPLC. The first used a Zorbax Sax analytical anion exchange (ANX) column (4.6 mm x 250 mm) on an Agilent 1200 series instrument with a

quaternary pump and UV detection at 254 nm. Solvents for elution included (A) water and (B) 0.5 M sodium chloride. At a flow of 1.0 mL/min, the gradient was (1) 100% A for 6 min then (2) 100 % B for 22 min (Figure 5.2).

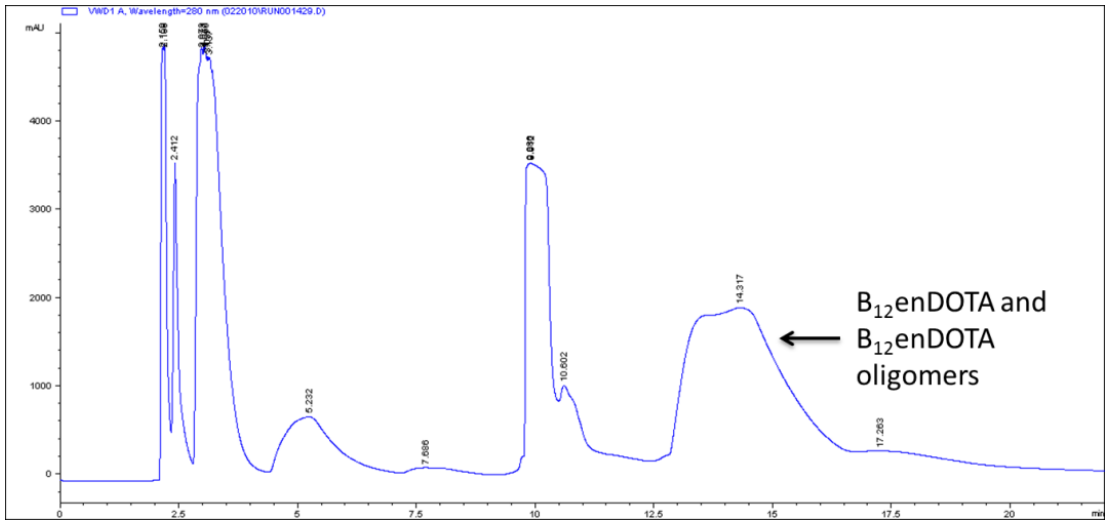

Figure 5.2. ANX Purification of 1 by RP-HPLC, with elution of 1 beginning at 13 min.

Each peak was collected and characterized by MALDI-ToF/MS, which suggested that the ANX HPLC peak with a retention time of 13–14.5 min was **1** (showing major MALDI-ToF/MS peaks at 1801.7 m/z, indicative of $[M^+–CN]$). However, this peak also showed MALDI-ToF/MS peaks at 2770.1 m/z, and 3198.3 m/z, suggesting that other impurities had eluted with the **1**, including $B_{12}enB_{12}$ and $B_{12}enDOTAenB_{12}$. The target peak was dried *in vacuo* and redissolved in H_2O (0.1 % TFA) to uniformly protonate the three unbound carboxylic acid arms of DOTA in preparation for a second C_{18} RP-HPLC purification to isolate **1** from the ANX impurities.

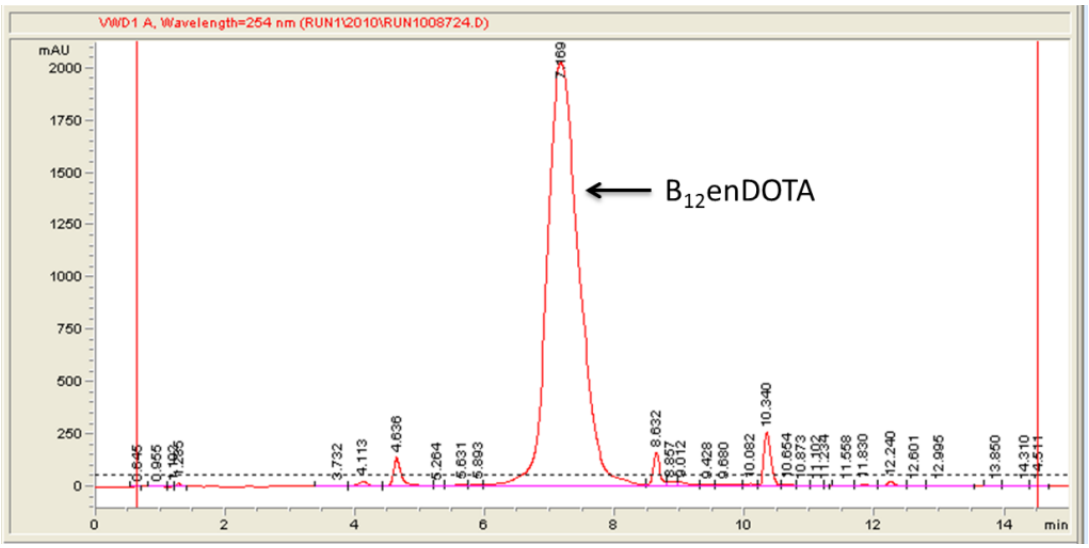

Figure 5.1. C_{18} Purification of B_{12}enDOTA (1) by RP-HPLC, with elution of B_{12}enDOTA (1) at 7.17 min.

The second purification was performed using a Zorbax C_{18} analytical column (42 mm x 10 mm) at a flow rate of 1.0 mL/min. Solvents for elution included (A) H_2O (0.1 % TFA) and (B) MeCN (0.1% TFA). The method was a linear gradient of 10% B to 20% B over 10 min. Under this method, **1** showed a T_r= 7.17 min (Figure 5.3). This peak was collected and dried *in vacuo*for characterization. The yield of **1** was ~11% based on B_{12}.

5.3.3 Characterization of 1

Purity of **1** was confirmed via ^{1}H NMR and MALDI-ToF/MS. An ^{1}H NMR spectra, taken in deuterium oxide (D_2O) at 300 MHz, confirmed the proposed structure of **1** and showed a downfield shift of the ethylene protons of DOTA. ^{1}H NMR peaks (in δ) included: 7.306 (1H, s), 7.126 (1H, s), 6.517 (1H, s), 6.361 (1H, s), and 6.111 (1H, s) (Figure 5.4).

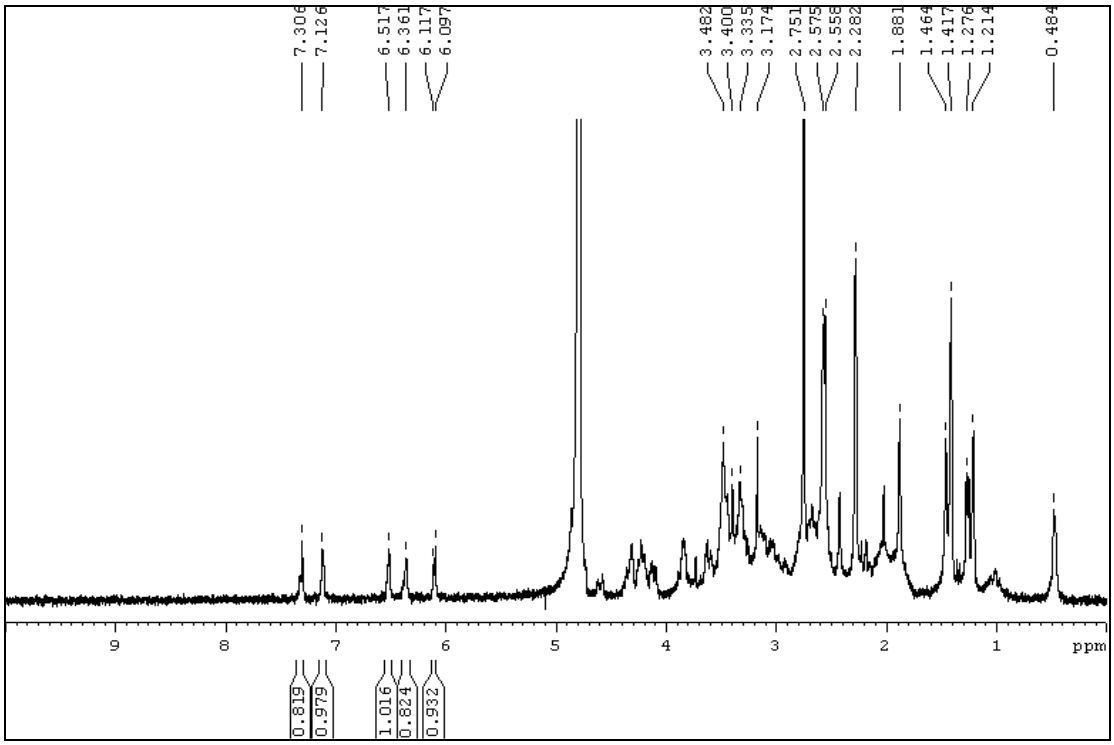

Figure 5.4. ^{1}H NMR of 1 in D_2O at 300 MHz.

The MALDI-ToF/MS of the HPLC peak at T_r= 7.17 min contained a peak at 1801.7 *m/z*, consistent with the theoretical molecular mass of $[M^+]$ = 1827.9 minus the cyano group of cyano-B_{12}, $[M^+–CN]$ = 1802.08 *m/z* (Figure 5.5). The isotopic distribution pattern of this peak was consistent with that of the calculated isotopic distribution pattern of **1**, based on the formula $C_{82}H_{120}CoN_{20}O_{22}P$ (Figure 5.6).

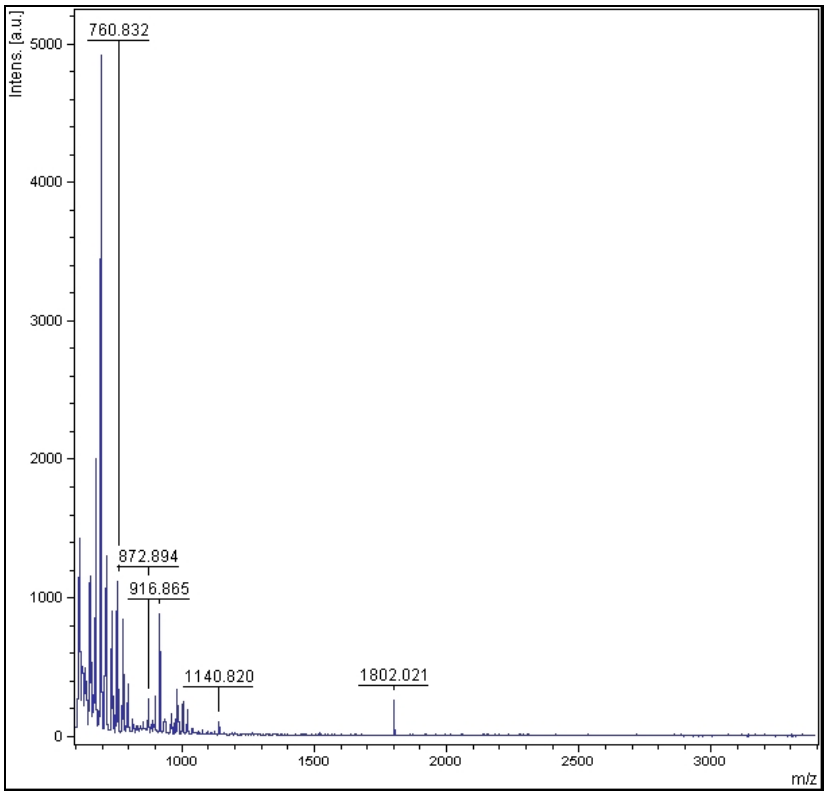

Figure 5.5. MALDI-ToF/MS showing a peak at 1802 *m/z* consistent with 1 without the cyano group of B_{12}.

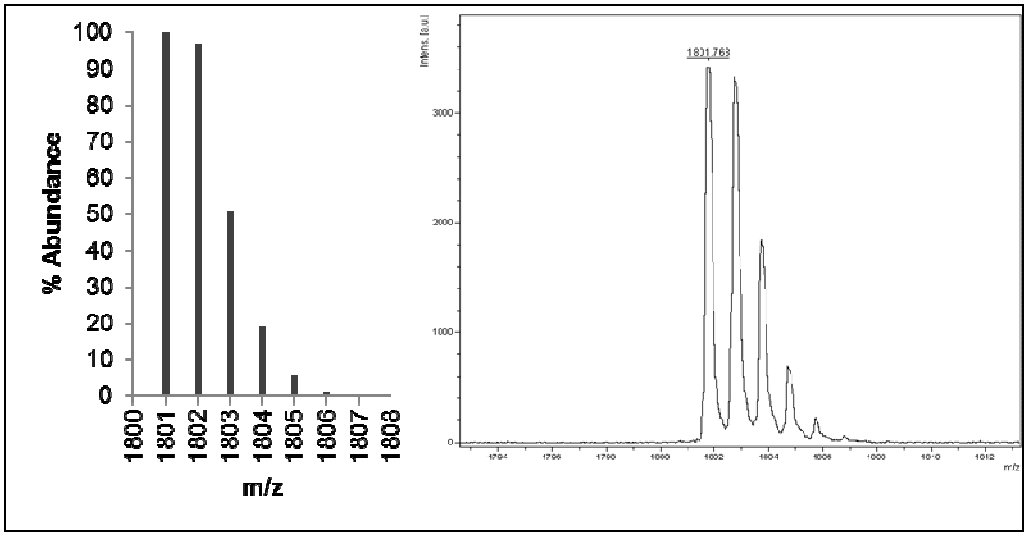

Figure 5.6. Calculated (left) and experimental (right) isotopic patterns of 1, without the cyano group of B_{12}, are equivalent.

The RP-HPLC trace showed an impurity, represented by a second peak with T_r=5.11 min. This peak was confirmed by MALDI-ToF/MS to be **1** with a proton captured within the DOTA macrocycle, 1801.1 m/z. An experiment at 65°C confirmed the proton adduct theory, as the peak disappears in the RP-HPLC trace when the proton is driven out of DOTA in higher temperatures.

5.3.4 Radiolabeling of 1 with ^{64}Cu for *In Vivo* Uptake Studies

A pure sample of **1** was sent to Dr. Suzanne Lapi and Dr. TayoIkotun of the Department of Radiology at Washington University in St. Louis, MO, for radiolabeling. **1** was labeled with ^{64}Cu to give ^{64}Cu-B_{12}enDOTA (**2**). At 23 °C, both **1** and the impurity at T_r= 5 min (discussed in section 5.3.3) were labeled (Figure 5.7). **1** was labeled at 95% efficiency by radiation counts.

At 65 °C, **1** was labeled with ^{64}Cu at 100% efficiency, and the impurity was no longer seen. As suggested above, it is likely that upon heating, the proton was driven out of the DOTA macrocycle and replaced by ^{64}Cu (Figure 5.8).

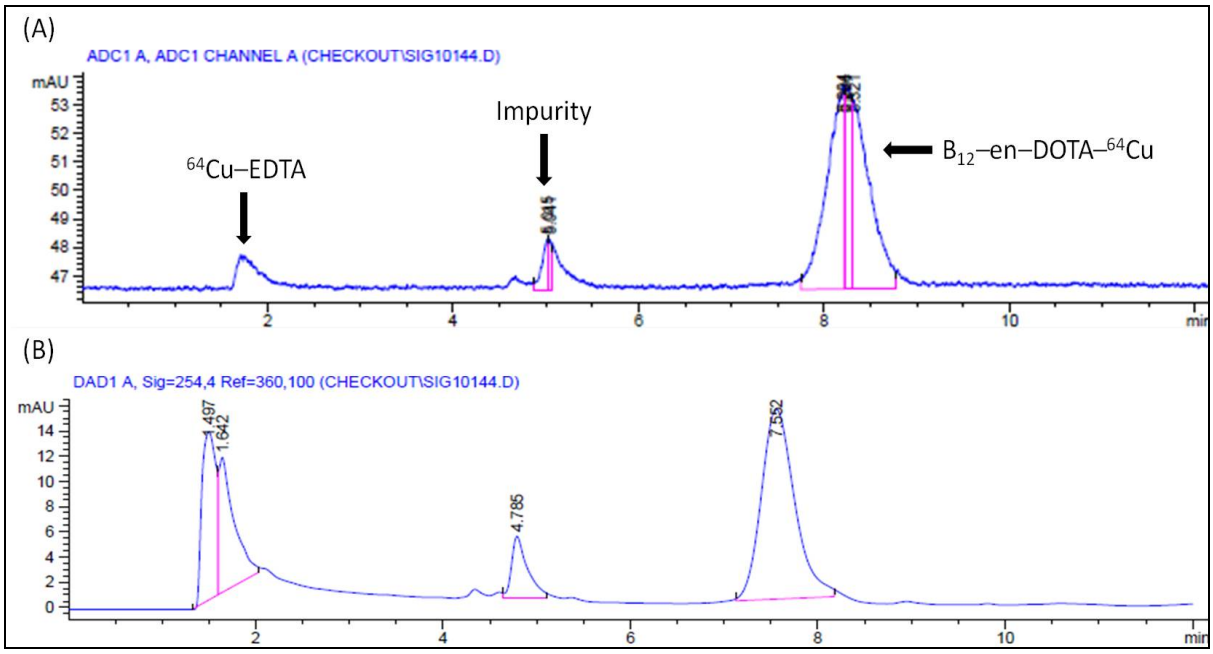

Figure 5.7. RP-HPLC chromatograph following ^{64}Cu labeling of 1 at 23 °C.

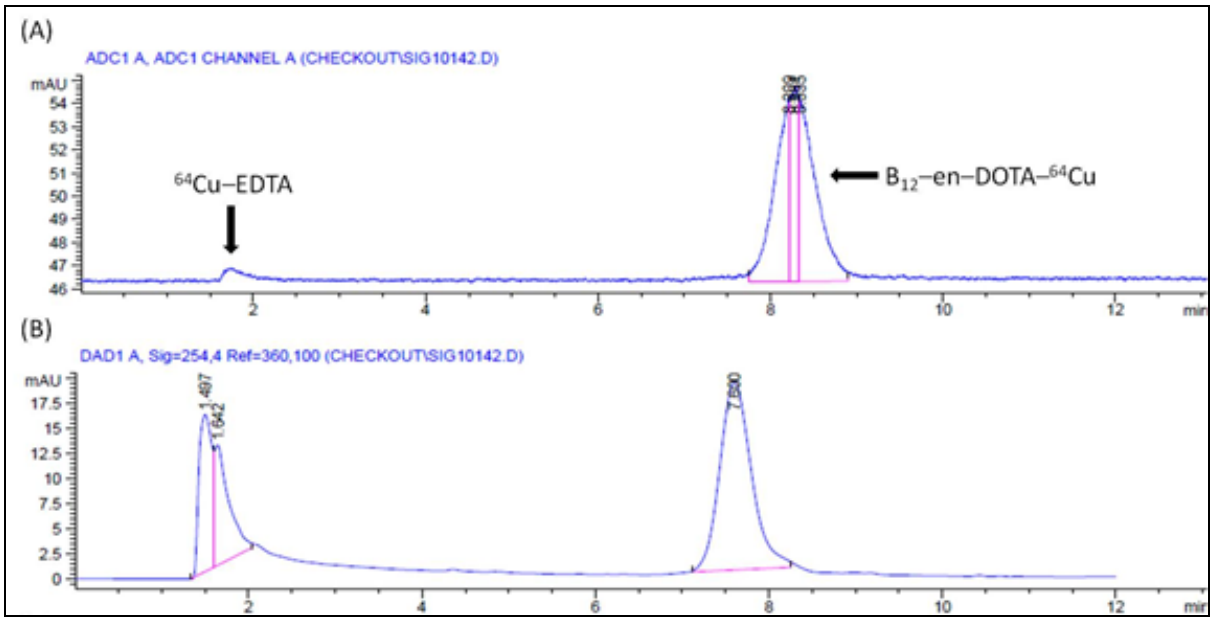

Figure 5.8. RP-HPLC instruments chromatograph following^{64}Cu labeling of 1 at 65 °C. At 65 °C, the impurity at T_r= 5 min disappears and 100% labeling is achieved.

5.3.5 Preliminary *In Vivo* Characterization of 2 in a Mouse Model

2 was tested on two different cell lines transplanted into mice. The first, B16 mouse melanoma cells, were chosen because they are commonly used to study *in vivo* cancer targeting agents. In addition, these cells express membrane-associated HC *de novo*.[1] The second, human pancreatic cancer PaCa-2 cells, were chosen because have been shown to express transcobalamin CD320 receptor for TCII.[35] In combination, the B16 and PaCa-2 cell lines allowed for the study of the specific HC and TCII B_{12} uptake mechanisms, respectfully.

Two groups of mice were placed on a B_{12} deficient diet over a period of two weeks and implanted with either B16 or PaCa-2 cells. The cells were allowed to grow for up to two weeks. **2** was injected intravenously, and the biodistribution was determined at 6 and 24 h by isolation of mouse organs and conduction radio counts. The results for the B16 are shown in Figure 5.9, and the results for the PaCa-2 cells are shown in Figure 5.10.

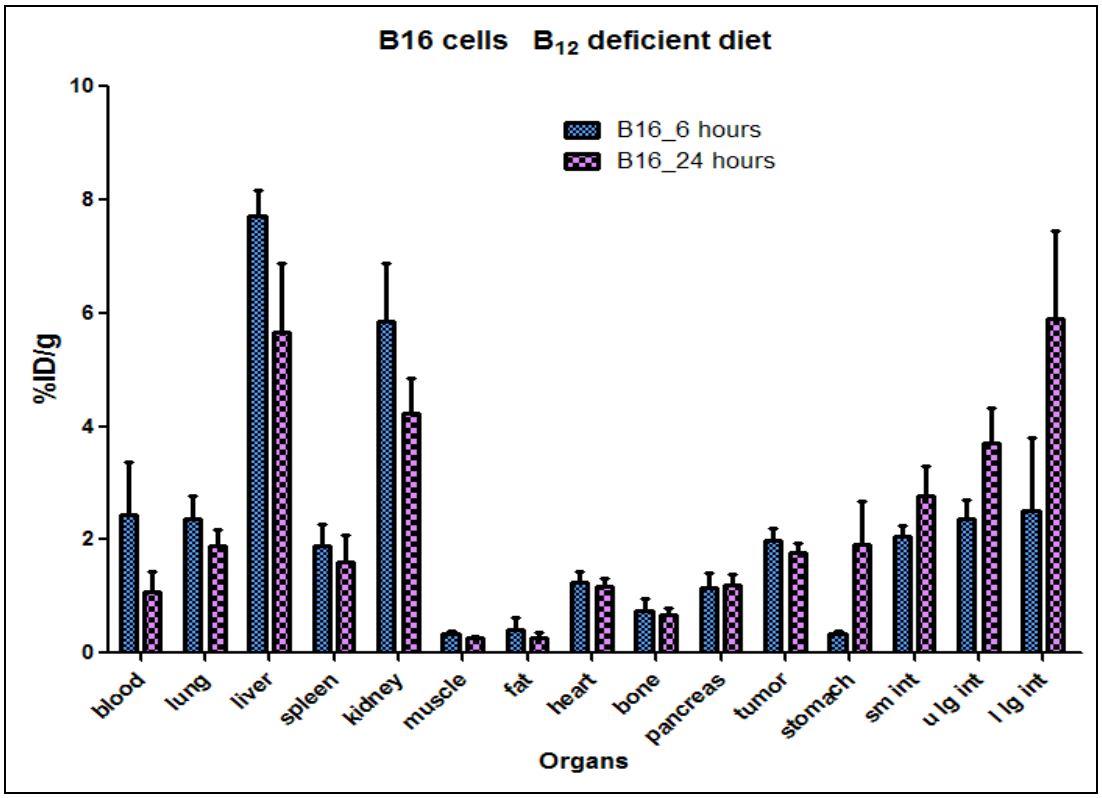

Figure 5.9. Biodistribution of radiation counts 6 and 24 h after injection of 2 into mice with B16 cell tumors, which express membrane-bound HC *de novo*.

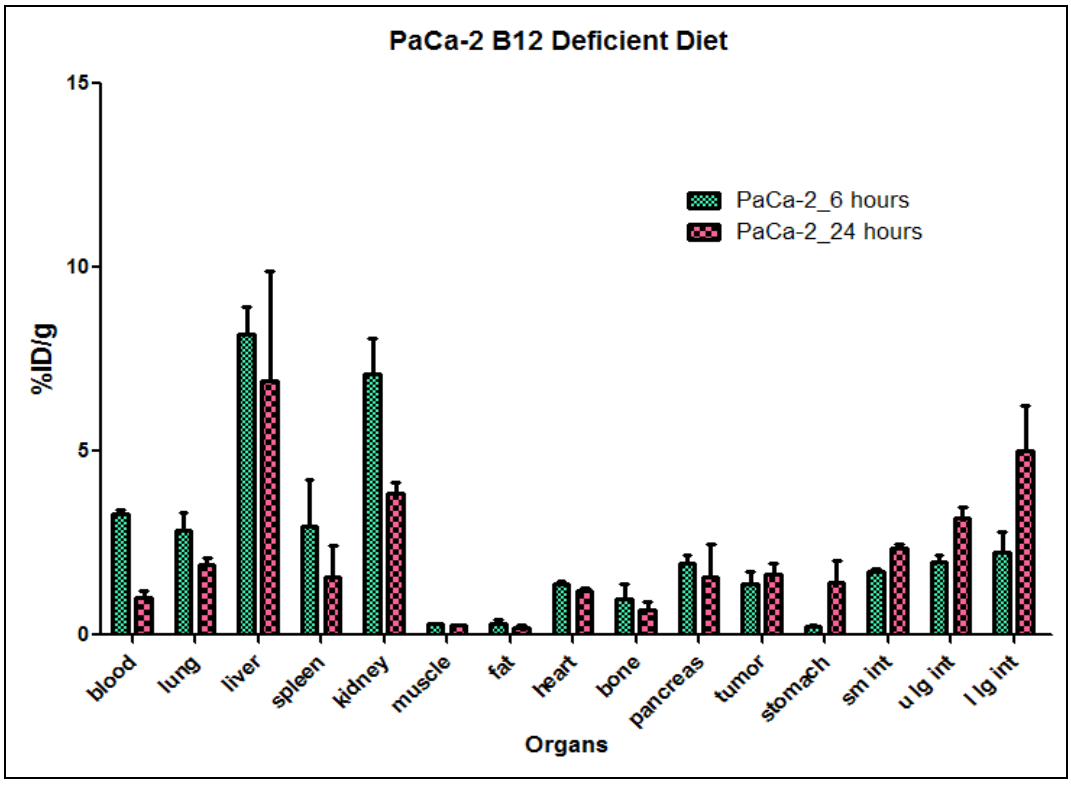

Figure 5.10. Biodistribution of radiation counts 6 and 24 hr after injection of 2 into mice with PaCa-2 cell tumors, which are known to express TCII receptors.

In both tumor models, **2** showed about a 2% tumor distribution. A tumor distribution of at least 5% would be ideal. However, at 2% tumor distribution, **2** was successful in visualizing the PaCa-2 tumor. In order to demonstrate that? **2** was targeting the cells through a B_{12} receptor, excess free B_{12} was added to saturate the B_{12} receptors and block distribution. Figure 5.11 shows the successful visualization of the PaCa-2 tumor (left) and block of **2** through the addition of excess free B_{12} (right).

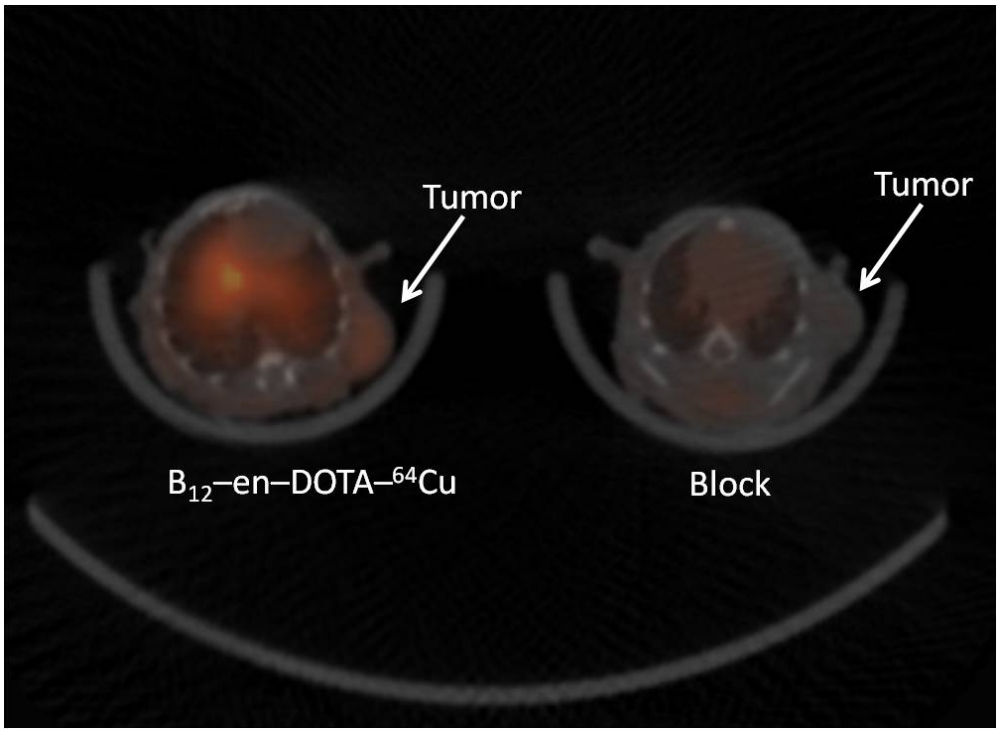

Figure 5.11. Left: The PaCa-2 tumor is visualized by intravenous injection of 2. Right: Addition of free B_{12} blocked delivery of 2, indicated that a B_{12} receptor had been targeted.

Outside of the tumor, significant levels of radiation were detected in the liver, kidney, and small and large intestine. The high kidney distribution was expected due to a) the kidneys' role in clearing the drug and b) the high amounts of B_{12} receptors present in the organ. However, the high distribution in the liver and intestines warranted further investigation. The high amount of radiation detected in the liver suggested that free ^{64}Cu had been released from the DOTA macrocycle*in vivo*, a phenomena that has been reported in literature.[34] In response to the poor stability of **2**, a more stable conjugate incorporating a related ligand was synthesized (see Section 5.4). The high distribution in the small and large intestine suggested that the animals were actually re-digesting fecal matter

containing the cleared radiolabeled drug during the experiment. In order to prevent this, metabolic cages will be used in future experiments to prevent ingestion of fecal matter. It is hypothesized that in future experiments, incorporating the new conjugate and metabolic cages, a tumor distribution of higher than 2% can be achieved.

5.4 B_{12}en(*S*)-*p*-SCN-Bn-1,4,7-triazacyclononane-*N*,*N′*,*N″*-triacetic acid (B_{12}enNOTA)

A more stable chelator molecule was selected for a revised probe construct. A related macrocyclic ligand, 1,4,7-triazacyclononane-*N*,*N′*,*N″*-triacetic acid (NOTA), was substituted for the DOTA, to give an optimized compound, B_{12}enNOTA (**3**) with a higher expected degree of kinetic stability in regards to chelating the ^{64}Cu. Thus, trials with **3** were expected to show less radiation in the liver.

5.4.1 Synthesis of 3

In the interest of maximizing reaction yield, the NOTA ligand was prepared with a thiocyanate group that is highly reactive with previously prepared B_{12}en. Mole equivalents of B_{12}en (20 mg, 1.38 x 10^{-2}mmol) and *p*-SCN-NOTA (6.21 mg, 1.38 x 10^{-2}mmol) were dissolved in 3 mL of 100 mM sodium carbonate, pH 10.5, and combined at room temperature. The reaction was left stirring under air for 16 h (Figure 5.12).

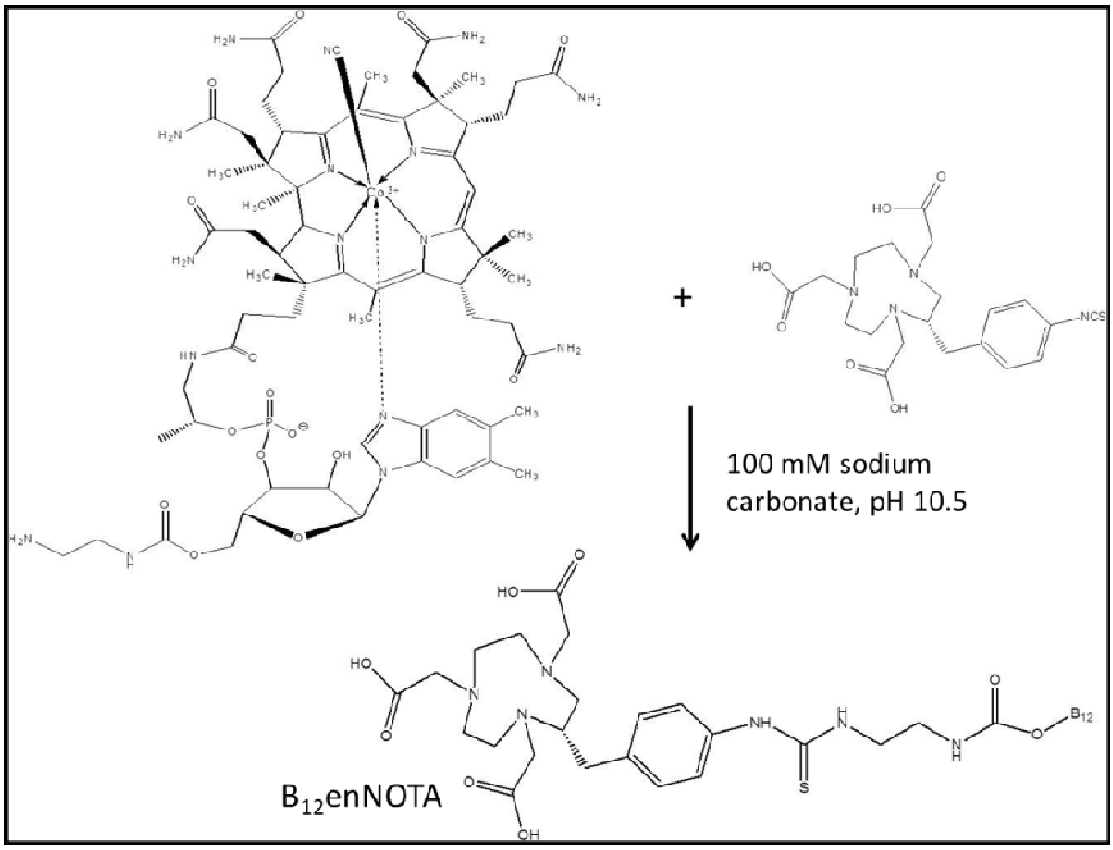

Figure 5.12. Coupling of B_{12}en to *p*-SCN-NOTA to give 3. The thiocyanate group helped increase yield.

5.4.2 Purification of 3

3 was purified by RP-HPLC using an analytical C_{18} column (4.6 mm X 150 mm, 3 µm particle size) on an Agilent 1200 series instrument with a quaternary pump and UV detection at 360 nm. The solvents for purification included (A) 0.1% TFA/water and (B) MeCN, and the flow rate was 1 mL/min. The method was a gradient of 10-25% B over 0-15 min. Under these conditions, B_{12}en eluted at about 7 min and **3** eluted at 12.5 min (Figure 5.13). The peak with R_t= 12.5 was collected and dried *in vacuo*for characterization. The yield was 95%.

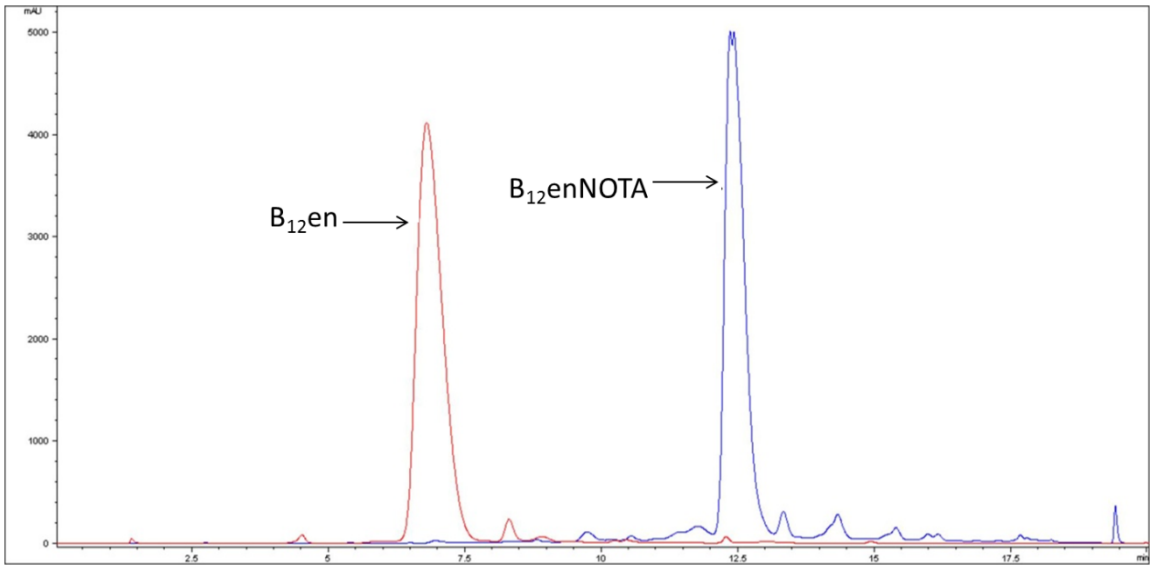

Figure 5.13. Purification of 3 by RP-HPLC, showing distinct elution of B_{12}en at ~7 min (red) and elution of 3 at ~12.5 min (blue).

5.4.3 Characterization of 3

The identity of **3** was confirmed by ^{1}H NMR, infrared spectroscopy (IR), and MALDI-ToF/MS. A ^{1}H NMR was taken in D_2O at 300 MHz, giving peaks (in δ) at: 7.283 (s, 2 H), 7.160 (s, 2 H), 7.096 (s, 1 H), 6.455 (s, 1 H), 6.276 (d, 1 H), 6.00 (t, 1 H).

In the coupling reaction, the isothiocyanate group of the *p*-SCN-NOTA would disappear; IR spectroscopy was utilized to look for the absence of the intense characteristic isothiocyanate stretch at 2125 cm^{-1}. The IR confirmed that this band was gone, and thus that the original reactant containing the group, the *p*-SCN-NOTA, had fully reacted with the B_{12}en (Figure 14). In MALDI-ToF/MS, the mass of **3** $[M - CN]^{+}$ was expected to be 1867 *m*/*z*. Figure 5.15 shows a peak

at 1867.483 *m/z,* confirming the identity if **3.**

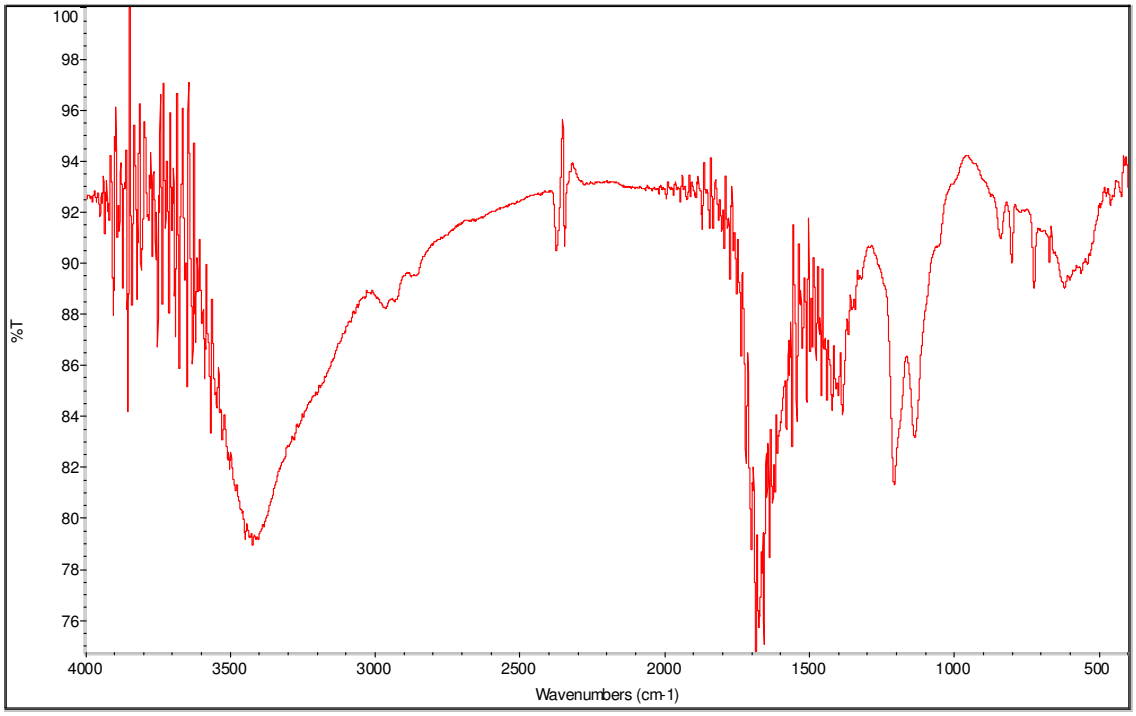

Figure 5.14. IR spectrum of 3, showing a lack isothiocyanate group, represented by a band at 2125 cm^{-1}.

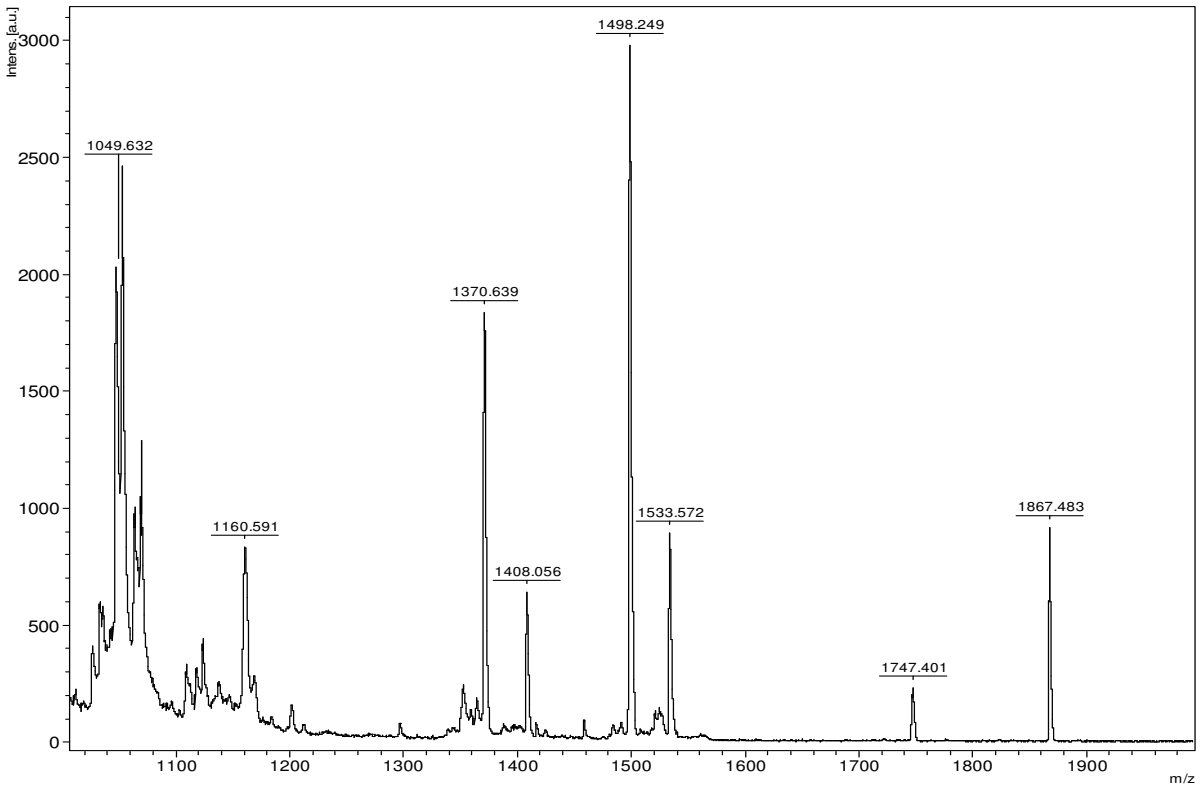

Figure 5.15. MALDI-ToF/MS showing a peak at 1867 *m/z*, consistent with 3 without the cyano group of B_{12}.

5.5 Future Work

It is hypothesized that the tumor distribution of a radiolabeled B_{12} probe will be increased by the incorporation of the NOTA ligand and inclusion of metabolic cages in the animal protocol. The increased stability of the NOTA chelate for the ^{64}Cu is expected to lower radiation in the liver, while the prevention of fecal ingestion is expected to lower radiation in the small and large intestine. These experiments are currently underway in collaboration with Dr. Lapi and Dr. Ikotun at Washington University.

6 B_{12} Monocarboxylic Acid Derivatives

6.1 Introduction

While B_{12}-based imaging agents have experimentally labeled tumor tissue through successful receptor-mediated endocytosis of the TCII-bound B_{12} conjugate,[35] significant background levels of radioactivity were detected in normal tissue.[1] In particular, high uptake is seen in the kidneys and the liver because these organs are responsible for clearing and storing B_{12}, respectfully.[1] High uptake of radiolabeled compounds in the kidney may lead to radiation toxicity, and the radiation dose to the kidney is often the "dose-limiting" factor for the clinical use of nuclear medicine.[1]

However, the highest expression of CD320 is seen in the kidneys, which poses a problem for the development of B_{12}-based therapeutics. A solution to this problem would be to knock out the B_{12} conjugate's ability to bind with TCII, yet maintain binding with other important transport proteins. Additionally, Waibel et al. suggest that a B_{12}-based probe with decreased binding with TCII would clear from the blood more quickly than the transport protein-bound form, decreasing overall systemic toxicity.[1]

In response to the demand for a more specific imaging agent, there has been a focus on synthesizing B_{12}-based probes incorporating monocarboxylic acid derivatives of B_{12} (MCAs). Mild acid hydrolysis of B_{12} produces a mixture of MCAs derived from the b, d, and e propionamide side chains; these side chains

are more susceptible to the hydrolysis than the a, c, and g side chains.[1] While the MCAs retain vitamin function and normal interaction with HC, modification certain propionamide side chains affects B_{12}'s ability to bind with TCII, decreasing relative affinity by less than a factor of 10 for conjugates of the *b*-isomer of the MCA.[1,2] By disrupting the binding of B_{12} to its transfer protein TCII and inhibiting uptake by TCII receptors, building B_{12}–based conjugates incorporating MCAs are ideal to prevent non-targeted organ uptake and target the cancer cells that express HC *de novo* with a high signal-to-noise ratio.[1]

6.2 Synthesis of MCAs

Marques and Scooby investigated the optimal reaction conditions for the generation of MCAs, reporting that maximum conversion (42% yield) of B_{12} to the *e, b,* and *d* MCA isomers occurred in 1 M hydrochloric acid (HCl) at 50°C for 2 hours.[36]

B_{12} (cyanocobalamin, 50 mg, 36.9 mmol) was dissolved in 5mL of 1 M HCl and allowed to react for 2 h at 50°C (Figure 6.1). The reaction was neutralized with 1 M sodium hydroxide (NaOH) and loaded on Amberlite ion exchange resins for desalting. The reaction was eluted from the resins in 100% MeOH, dried *in vacuo,* and redissolved in 10 mL H_2O.

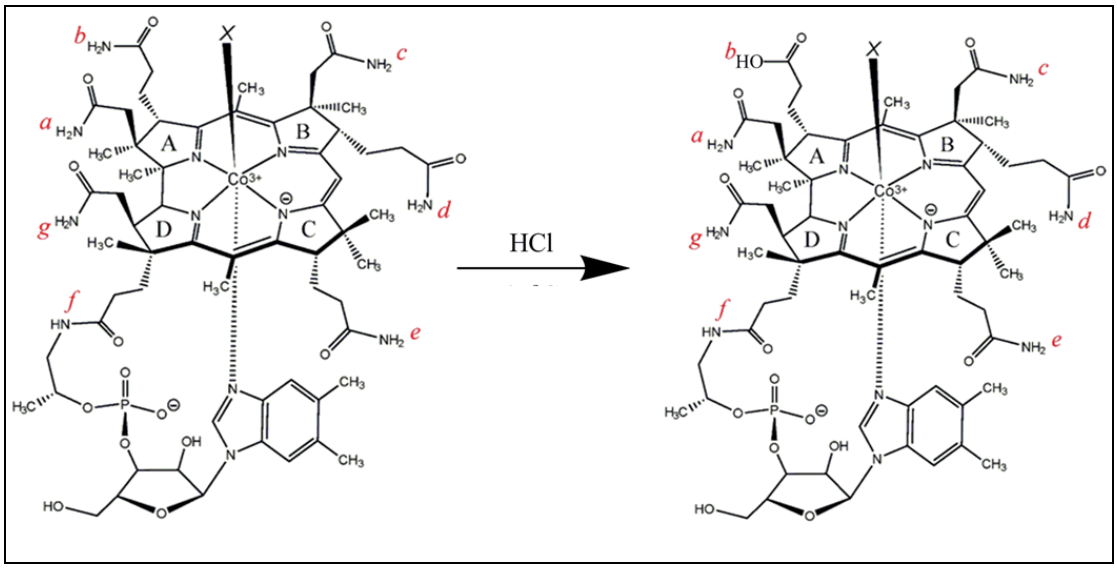

Figure 6.1. The conversion of B_{12} to B_{12} MCA via acid hydrolysis (the *b*-acid isomer is shown).

6.3 Purification of MCAs

The crude reaction was purified by fast protein liquid chromatography (FPLC) using a 5 mL diethylaminoethyl (DEAE) Sepharose Hi Trapanion-exchange column chromatographyon an AKTA prime plus liquid instrument with an automated fraction collector and UV detection at 280 nm (GE Healthcare). All runs were carried out at 4°C. The reaction was filtered through a 0.64µm filter and loaded at 0.5 mL/min in 100% H_2O. After the initial flow-through peak (confirmed by MALDI-TOF/MS to be unreacted B_{12}), the MCAs were eluted at 2.5 mL/min at 2% 1 M NaCl and collected as a single fraction for subsequent purification by HPLC. B_{12}-dicarboxylic and tricarboxlic acids (confirmed by MALDI-TOF/MS) were eluted together at 100% 1 M NaCl (Figure 6.2).

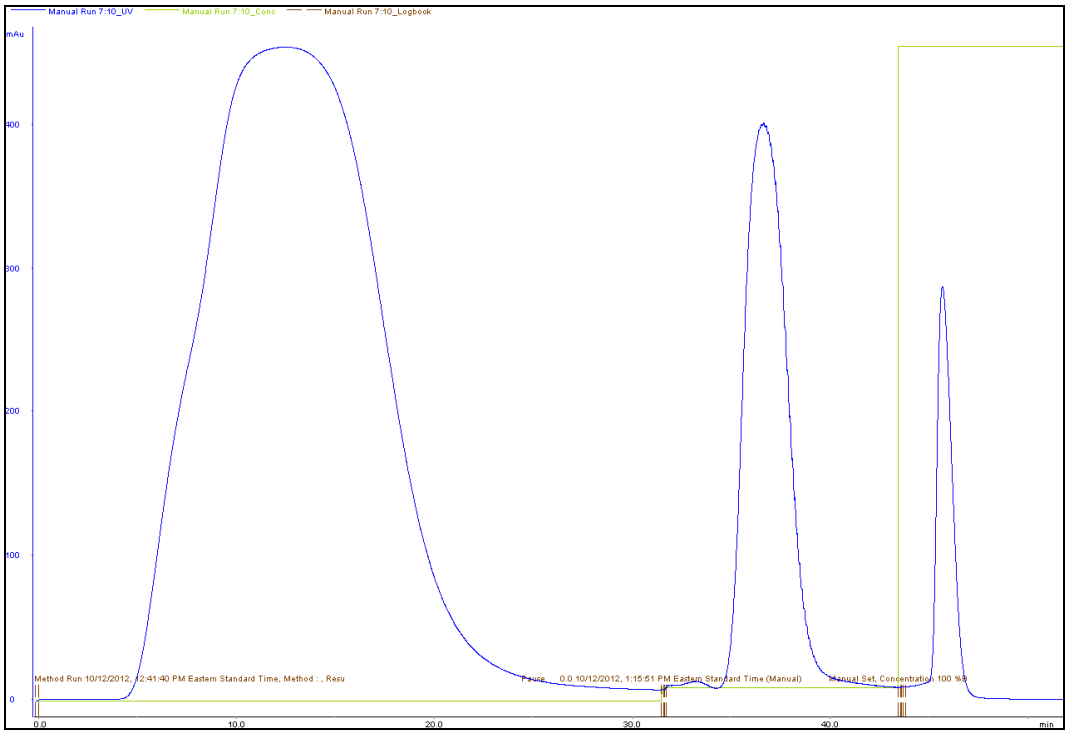

Figure 6.2. FPLC trace of crude B_{12} MCA reaction. The MCAs elute at 2% 1 M NaCl in the second peak at 36 min.

The peak that eluted at 2% 1 M NaCl (36 min) was dried *in vacuo* and redissolved in 5 mL H_2O for a second purification by reversed-phase high-performance liquid chromatography (RP-HPLC) using an Semiprep Eclipse XDB-C18 column (9.4 mm X 250 mm, 5 µm particle size) (Agilent Technologies, Santa Clara, CA) on an Agilent 1200 series instrument with a quaternary pump and UV detection at 360 nm. This purification was optimized to separate the MCA isomers.

The solvents that were used for elution included (A) 50 mM phosphate buffer pH 6.5 and (B) MeCN. At a flow rate of 3.0 mL/min, the gradient was (1) 5–15% B over 0–15 min, (2) 15% B for 15-20 min, (3) 15–50% B over 20-26

min, and (4) 50–5% B over 26–32 min. The trace is shown in Figure 6.3. Three prominent peaks at T_r=14.89 min, 15.87 min, and 17.12 min were collected, dried *in vacuo,* and loaded on Amberlite ion exchange resins for desalting. Each peak was eluted from the resins in 100% MeOH, dried *in vacuo,* and characterized by MALDI-ToF/MS and 2D Heteronuclear Single Quantum Coherence NMR (2D NMR HSQC).

6.4 Characterization of MCAs

The purity of the MCAs were confirmed by MALDI-ToF/MS, with significant peaks seen at 1330.6 *m/z* [M^+ - CN] and 991.4 [M^+ -CN-base-sugar-PO_4]. Unreacted B_{12} from the reaction gave related yet distinctly different peaks at 1329.6 *m/z* [M^+ - CN] and 990.5 [M^+ -CN-base-sugar-PO_4].

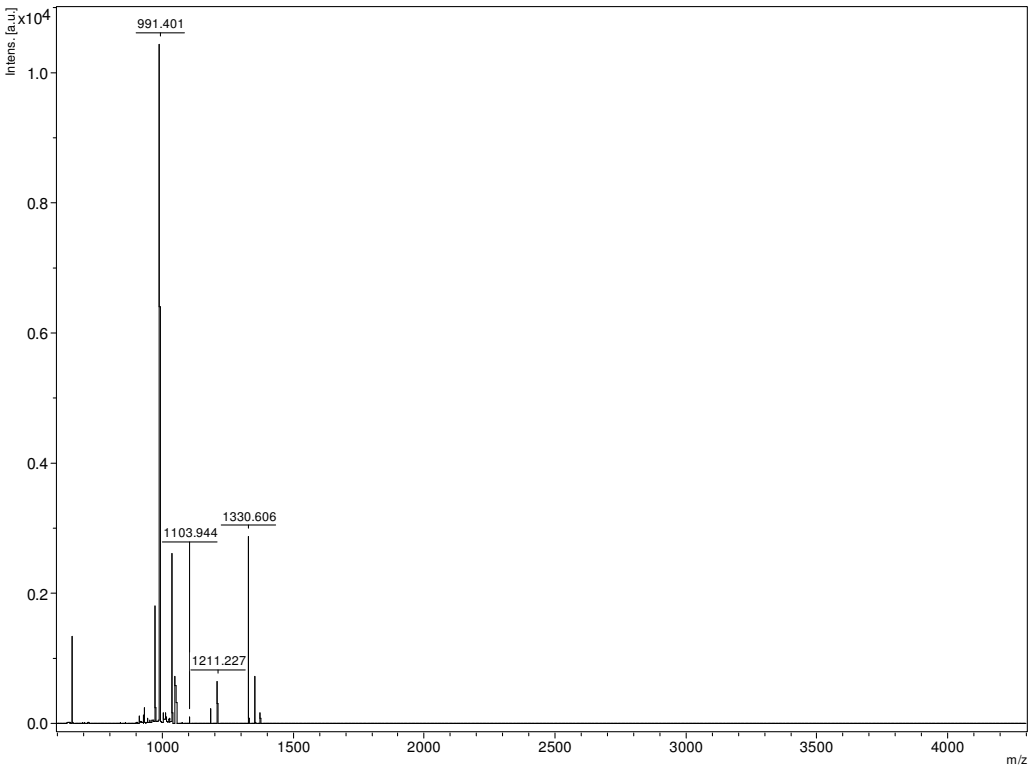

Figure 6.3. MALDI-ToF/MS spectrum of peak 3 from RP-HPLC.

Isomer assignments, based on 2D NMR HSQC taken in deuterium oxide (D_2O), were: Peak 1 (T_r=14.89 min) as B_{12} e-MCA, Peak 2 (T_r= 15.87 min) as B_{12} d-MCA, and Peak 3 (T_r= 17.12 min) as B_{12} b-MCA. These assignments are consistent with literature.[36] The yields (by mass) of each isomer are reported in Table 6.1.

MCA Isomer	RT-HPLC Retention Time (T_r) in min	Yield
e-acid	14.89	13.9%
d-acid	15.87	12.5%
b-acid	17.12	15.1%

Table 6.1. Yield of RT-HPLC Purified MCA Isomers.

6.5 Future Work: Construction of B_{12} MCA Probes

Because the MCAs bind only to HC, it is hypothesized that MCA-based probes will demonstrate improved *in vivo* selectivity and lower systemic toxicity. The *in vivo* probes B_{12}enDOTA and B_{12}enNOTA described in Chapter 5 will be reconstructed using the *b*-MCA isomer, tested in regards to binding affinity for TCI and TCII, and evaluated on animal models to compare background uptake in the kidneys and liver with the unmodified B_{12} conjugates. In addition, conjugation through this *b*-amide position could be used to generate a fluorescent B_{12}-MCA probe for use as a negative control in *in vitro* cell testing of B_{12}-based fluorescent probes, such as those described in Chapter 4.

7 Optimization of the B_{12} based fluorescent probe for *in vitro* cell screens via incorporation of lanthanide metals

7.1 Challenges of autofluorescence

While the B_{12}-ReThiazole probe described in Chapter 4 was used to successfully demonstrate the presence of the cubilin receptor in a lung cancer cell line, the probe was limited by its weak fluorescent signal. In general, light scattering, reflection, and autofluorescence are all problems associated with normal fluorescence microscopy, which can decrease the sensitivity and contrast of the probe signal.[37] In particular, the emission of the fluorescent B_{12}-ReThiazole was difficult to distinguish from background fluorescence of molecules naturally present in the cell.[38] This natural fluorescence that is seen in living tissue cultures is due to substances like flavins and porphyrins, which are all aromatic compounds that also are excitable in the by wavelengths used to excited the fluorophore region.[38]

A solution to this problems associated with fluorescent probes is to use phosphorescent molecules that exhibit delayed luminescence, allowing for the temporal separation of signals.[39] Figure 7.1 depicts a simple Jablonski diagram, which can be used to illustrate the difference between fluorescence (2) and phosphorescence (3) in terms of the electronic and vibrational states of a molecule; the processes differ in the way that electrons behave when excited by a photon. In both cases, when a molecule is excited with a photon, electrons move from the lowest energy conformation, the ground state, to a state of higher energy,

and then relax to the ground state via the emission of a photon. In fluorescence, the electron is excited to the lowest singlet excited state, and it relaxes to the ground state without undergoing any spin changes with a decay time of milliseconds.[40] By contrast, the electron in a phosphorescent system undergoes a spin flip that is "forbidden" by the quantum mechanical rules of electron transition; it is excited to the lowest triplet state and shows a much longer decay time on the order of seconds, or longer. As such, time-resolved spectroscopy can be adjusted to detect only the long-lived emission from the phosphorescent fluorophore.[41]

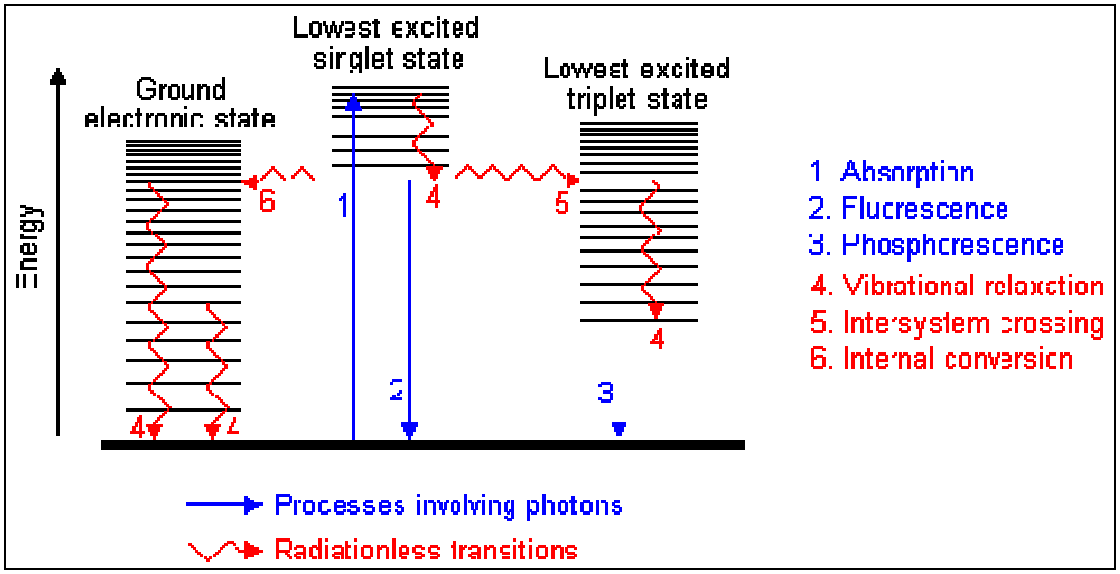

Figure 7.1. Jablonski diagram showing the difference between fluorescent emission (2) and phosphorescent emission (3). In the simplest case of fluorescence, the excitation wavelength is defined by photon 1, the electron is excited to the lowest singlet excited state, and the emission wavelength is defined by photon 2. In phosphorescence, the emission photon is photon 4.[42]

7.2 Lanthanides

The lanthanides (Ln) are the 15 elements from lanthanum to lutetium, located in the f series of the periodic table (Figure 7.2). Existing essentially in their trivalent state, Ln^{+3}, and bearing a [Xe]4fn electronic configuration, these 'hard' metal ions possess high charge densities and form electrostatic bonds. Ln ions display large and variable coordination numbers (CN = 6-12), with 8 and 9 often being the most common.[43] As 'hard' acids, the Ln ions show preferential binding to 'hard bases' such as oxygen, nitrogen or fluorine based ligands, rather than 'soft' bases such as phosphorous, sulphur, or iodine.[43]

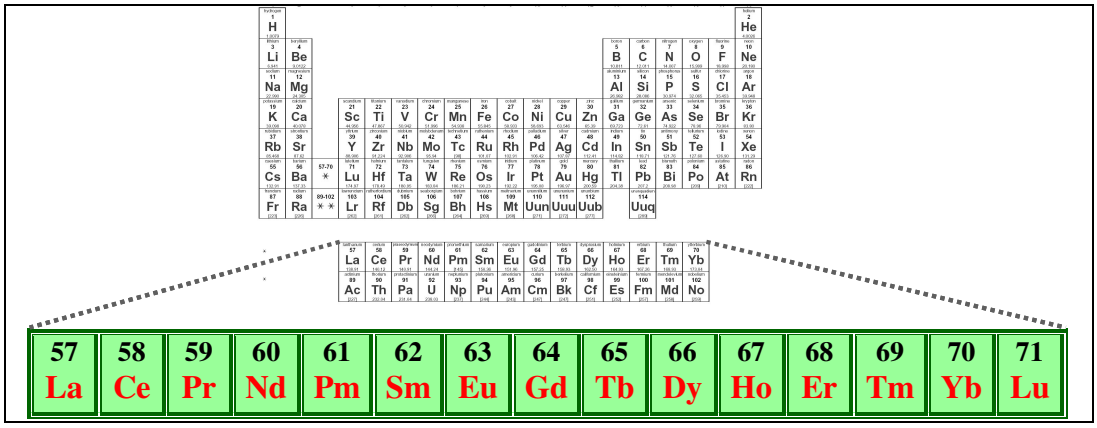

Figure 7.2. The lanthanides are found in the f series of the period table. Characterized by the gradual filling of their 4f orbitals, which are well shielded by the outer core 5s and 5p subshells, these "rare earth elements" display similar chemical resemblance but have very different physical properties.[43] Figure redrawn in: McMahon, B. Thesis. Trinity College Dublin. Dublin, Ireland. July 2011.

7.2.1 Lanthanides as Fluorophores

Scientists have looked towards the lanthanide metals as flurophores for biomedical analysis, medical diagnosis, and cell imaging.[44] The lanthanides exhibit long lived excited states (microseconds for YbIII and NdIII to milliseconds for EuIII and TbIII), and the delayed Ln luminescence can be clearly distinguished from the much shorter lived (sub-microseconds) background fluorescence, giving an improved signal-to-noise ratio for live-tissue work.[45] Figure 7.3 represents the time gating procedure for the detection of lanthanide luminescence, where excitation occurs via a pulsed lamp or laser, and measurements are taken after a programmed time delay, allowing the background luminescence to fade.[46] Luminescent Ln ions such as terbium (TbIII), europium (EuIII), samarium (SmIII), which have emissions in the visible region, and neodymium (NdIII), ytterbium (YbIII), holmium (HoIII), which have emission in the NIR region, have been used as diagnostic tools in biomedical analysis, shift reagents for NMR spectroscopy and as luminescent labels for fluoroimmunoassays.[43] GdIII, EuIII and TbIII are reported as the most emissive.

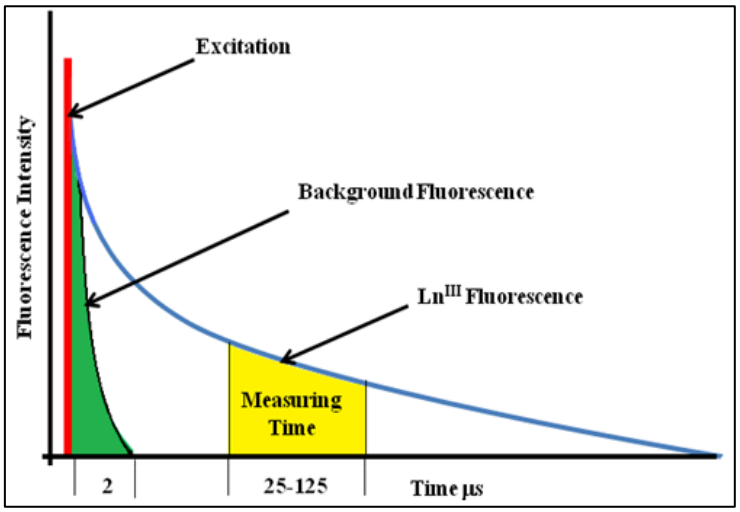

Figure 7.3. A graphical representation of the time-gating procedure displaying the long lived emission of the Ln ions (redrawn in: McMahon, B. Thesis. Trinity College Dublin. Dublin, Ireland. July 2011).

7.2.2 Indirect Excitation of Lanthanides via the Antennae Effect

In order to maximize the capability of Ln luminescence for fluorescence studies, their drawbacks must be recognized, and coordinating ligands designed to help overcome these obstacles.[44] A major problem in using these metal ions is the Laporte-forbidden nature of their f-f transitions, resulting in weak absorptions, with extinction coefficients of less than 4 $M^{-1}cm^{-1}$.[47] As a result, unless a laser excitation source or a high ion concentration is used, both of which present challenges for cell work, direct excitation of these ions rarely yields detectable luminescence.[47] One method used to overcome this problem is the indirect excitation of the Ln ion via the "antennae effect."[48]

The process by which the photophysical emission from the Ln metal is produced using a simple aromatic system like a phenyl or aromatic chromophore

is summarized in Figure 7.4, which shows a second Jablonski diagram including both the sensitizing antenna (Ar) as well as the lanthanide ion (Ln). The ground state sensitizing antenna (Ar) is excited to its singlet excited state (1Ar) when absorption of a photon of light of a suitable wavelength occurs. This energy can be transferred into the antennas triplet state (^{3}Ar) via a spin forbidden intersystem crossing that is made possible due to the presence of the heavy Ln ion and significant amounts of spin-orbit coupling occurs. Provided that the energy of the triplet state lies at least 1700 cm^{-1} above the accepting Ln energy level, subsequent population of the Ln excited state (*Ln) will occur via an intramolecular energy transfer (ET) process. This energy level requirement prevents any unwanted thermally activated back-energy transfer to the ^{3}Ar state which would occur if the energy gap was too small.[49] However, a compromise must be met, as if the energy distance between both levels is too large, successful population of the *Ln state would be hindered.[47]

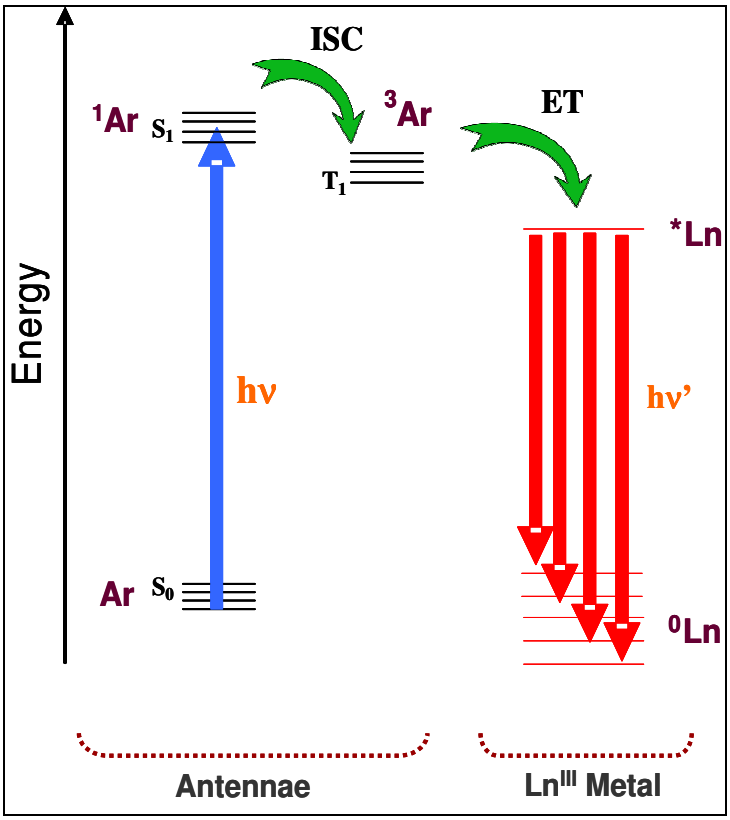

Figure 7.4. The sensitization of lanthanides via the antennae effect.[50] Figure redrawn in: McMahon, B. Thesis. Trinity College Dublin. Dublin, Ireland. July 2011.

To date, lanthanide complexes have been successfully synthesized and their usefulness in a variety of cellular studies has been demonstrated.[50] These complexes have been used as pH probes, anion or cation sensors, as well as for the imaging of biological materials. For example, McMahon et al. explored the use of a supramolecular Eu(III) complex as a bioprobe for selective imaging of microcracks in bones often caused by constant stress due to medical conditions like osteoporosis. The presented cyclen-based bioprobe was found to selectively bind to bone in exposed calcium(II) sites.[51] A cyclen-based Tb (III) bioprobe was

developed by Bornhop et al. to detect early-stage oral cancer lesions using a hamster model in vivo.[52] The incorporation of Eu(III) and Tb(III) in engineered cyclen framework holds extraordinary potential for the development of target-specific bioprobes that can be followed by their characteristic emissions.

7.3 Synthesis of cyclen-based lanthanide complexes for conjugation with B_{12}

It was hypothesized that replacing the rhenium metal with a lanthanide metal along with a suitable sensitizing chromophore would result in a more optimized B_{12}-based fluorescent system. In order to design and synthesize a Ln metal complex that maximized fluorescence and was suitable for B_{12} conjugation, a collaboration with Professor Thorfinnur Gunnlaugson lab group at Trinity College, Dublin was established. The synthesis of the final compound was carried out in a series of reactions, beginning with the synthesis of the chromophore and pendant arms, followed by the incorporation of the chromophore and special pendant arm into a cyclen molecule; the resulting macrocyclic compound was labeled with europium (EuIII) and terbium (TbIII) to give the target fluorescent system. Each reaction product was named with initials and a number.

7.3.1 Cyclen Framework

Other non-radiative and radiative pathways are in constant competition with the successful population of the *Ln excited state.[38] Examples of such processes include the radiative deactivation of the ^{1}Ar singlet excited state to the

Ar ground state resulting in molecular fluorescence production, non-radiative decay of the ^{1}Ar singlet excited state through collisions and vibrational interactions with surrounding molecules, or the non-radiative decay of the *Ln excited state through vibrational interactions with other molecules.[49] These de-activation processes can be minimized through the use of a rigid metal-ion environment, free of high-energy vibrations, that also protects the Ln ion from collisions with the solution molecules.[44] Thus, the most successful lanthanide complexes are based upon the cyclen framework, which forms kinetically inert and thermodynamically stable metal complexes (Figure 7.5).[44] Besides offering a high degree of stability, these ligands also fulfill the Ln high coordination number requirement, by providing potentially eight coordinating sites, four by the macrocyclicnitrogens and four by the flexible pendant arms.

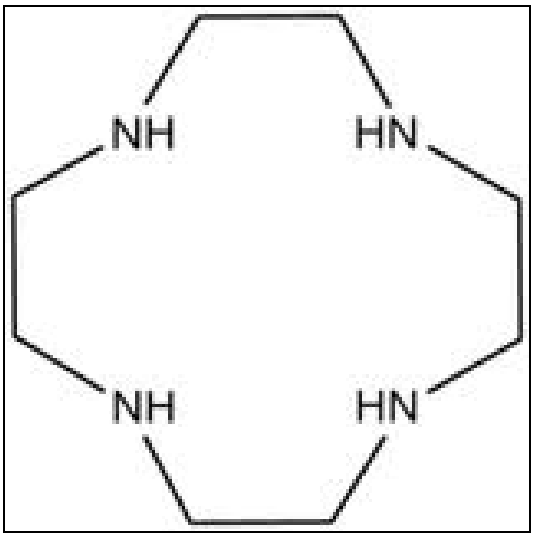

Figure 7.5. The cyclen molecule. As a ligand, cyclen provides a site to attach a variety of functional groups or ligands, allowing for the functionalization of the macrocyclic ring and the creation of a phosphorescent system suitable for a distinct biological role.[44]

7.3.2 1-aminoanthroquinone Chromophore

1-aminoanthroquinone was selected as the sensitizing chromophore. EuIII and TbIII, the two most rigorously studied emissive Ln metal ions, have excited states that lie at 17200 and 20500 cm^{-1}, respectively. Therefore, the chromophore needed to have an excited state 1700cm^{-1} above these values.[47] In addition, the molecule had an absorbance maximum at 360 nm, a wavelength compatible with the confocal microscope available. The structure of 1-aminoanthroquinone and the functionalization of the molecule via reaction with chloroacetyl chloride for future incorporation into the cyclen molecule are shown in Figure 7.6.

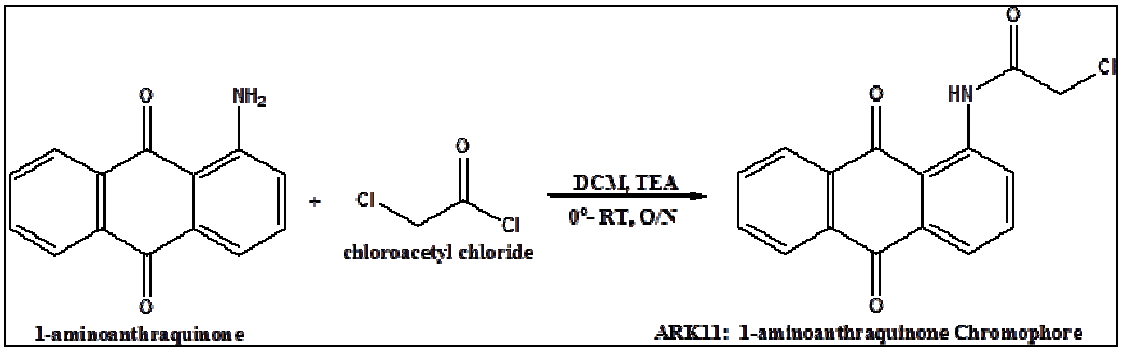

Figure 7.6. Synthesis of 1-aminoanthroquinone chromophore.1-aminoanthroquinone (1 g, 4.48 mmol, 1 equiv) was dissolved in 100 mL of DCM with triethylamine (0.49 g/0.69 mL, 4.93 mmol, 1.1equiv). The solution was cooled in a liquid nitrogen/ethanol bath. Chloroacetyl chloride (0.76g/ 0.54 mL, 6.72 mmol, 1.5 equiv) was added drop-wise to the solution over one hour. Reaction was left stirring overnight.

7.4 Preliminary Data

For cataloging purposes, the products of each reaction were named with the prefix ARK and a number that related the order in which they were synthesized. A peptide arm that offered both an ethyl ester-protected carboxylic acid for future coupling with B_{12}-ethylenediamine and a reactive chlorine for reaction with the nitrogen of the cyclen molecule was constructed by reacting glycine ethyl ester with chloroacetyl chloride; this arm was labeled ARK4. The functionalized 1-aminoanthroquinone chromophore was labeled ARK11. The cyclen-based complexes were synthesized in a series of reactions, beginning with a monoalkylation of the cyclen framework with the chromophore ARK11, followed by full alkylation with the peptide arm ARK4. An overview synthetic scheme for the unlabeled lanthanide complex, ARK15, is shown in Figure 7.7.

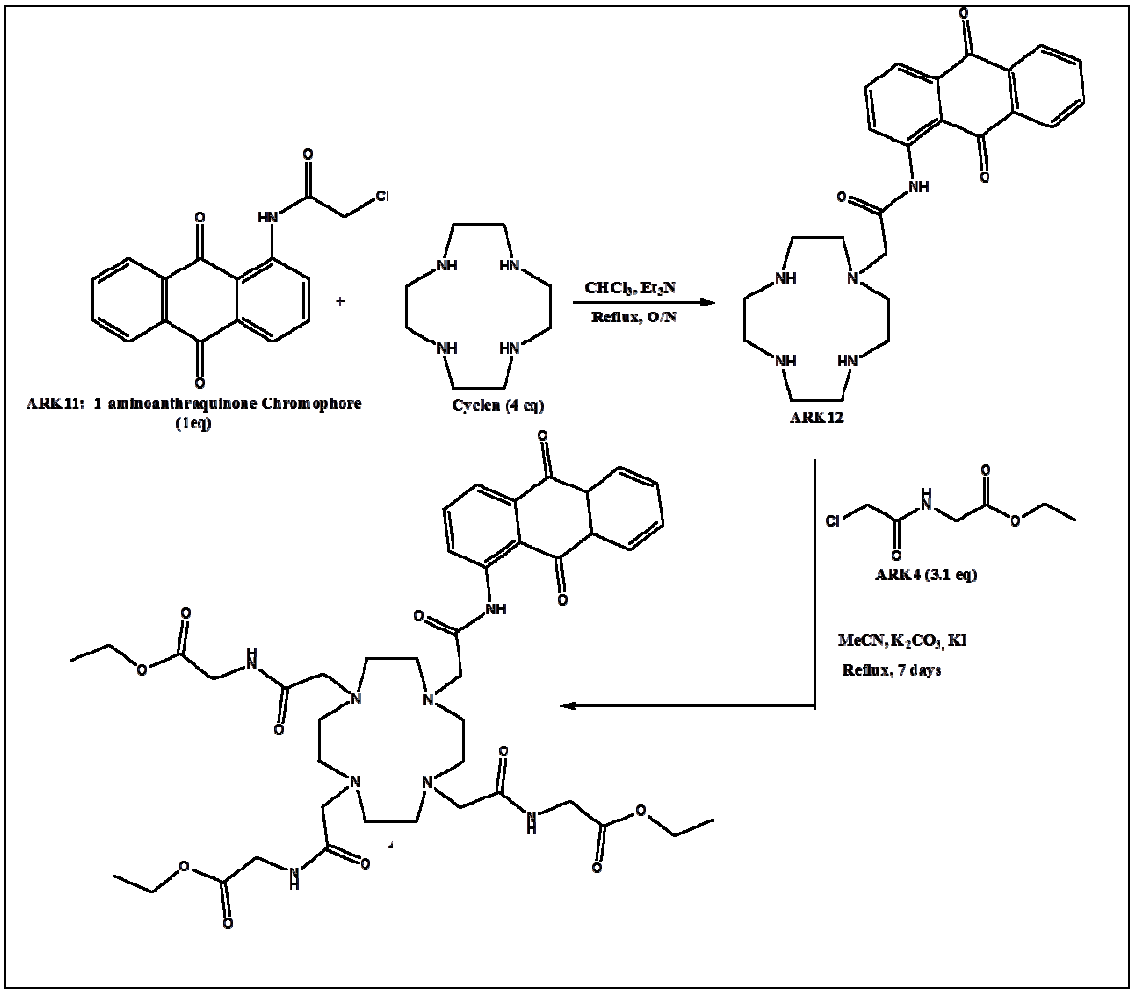

Figure 7.7. Synthesis of cyclen-based complex incorporating a 1-aminoanthroquinone chromophore and amino acid-based pendant arms (bottom left).

The compound ARK15 was labeled with europium and terbium to give the two distinct lanthanide complexes (Figure 7.8). The Ln metals were expected to be coordinated by the four nitrogen atoms of the cyclen molecule and the four oxygen atoms on each of the four arms.

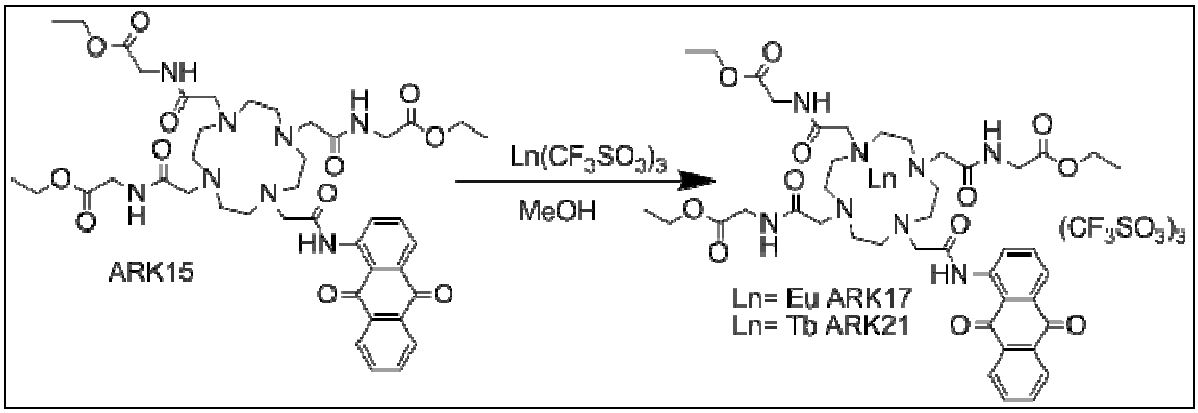

Figure 7.8. ARK15 (0.060 g, 0.070 mmol, 1 equiv) was dissolved in 14 mL of MeOH with 1:1 molar equivalent of europium triflate (ARK17) or terbium triflate (ARK21). The reaction was run in the microwave for 40 min at 70 °C.

After acid hydrolysis of the ethyl ester, the final lanthanide complexes were characterized by ^{1}H NMR, mass spectroscopy, and infrared spectroscopy. In addition, the complexes were characterized in terms of absorbance, extinction coefficients, phosphorescent emission, fluorescent emission, excitation spectra, and the lifetime. Based on the ^{1}H NMR, the final lanthanide complexes were not pure. While photophysical experiments showed characteristic emission bands for europium and terbium, the lifetime measurements suggested that the final product contained at least two distinct species with distinct quantum lifetimes.

7.5 Future work for cyclen-based lanthanide complexes

The lanthanide complexes must be purified and re-characterized by analytical and photophysical measurements. Once pure, the fully characterized lanthanide complexes will be conjugated to B_{12}-ethylenediamine via peptide

coupling to give an optimized fluorescent probe for *in vitro* confocal microscopy studies. In addition, these compounds can also be modified so that they may be used *in vivo.*

7.5.1 Conjugation with B_{12}

In order to advance the project, the purification must be optimized in order to yield pure samples of both the EuIII and TbIII compounds. Once isolated, each species can be characterized by ^{1}H NMR and MALDI-ToF/MS. Purified lanthanide complexes can then be conjugated with B_{12}-ethylenediamine, and then entire B_{12}-based lanthanide probe can be purified, characterized, and used in place of the rhenium probe as a means to screen cell lines for important B_{12} receptors.

7.5.2 Near-infrared (NIR)-emitting Lanthanides

The antennae moiety on the lanthanide complex can be exchanged to alter the emission profile of TbIII and EuIII, shifting visible emissions into the near-infrared region (NIR). Because NIR radiation can penetrate deep into sample matrices with low light scattering, NIR fluorescent materials show great potential for in vivo imaging of biological samples with a low background signal.[44] The system would be used in an *in vivo*, FRET-based detection system that would not require the use of X-rays or other potentially harmful forms of electromagnetic radiation.

8 Implications

One important route to new cellular probes and medical diagnostics with low toxicity that target rapidly dividing cancer cells is by exploiting these cells' voracious demand for nutrients. Using vitamin-based pathways for new diagnostics requires a biochemical and physiological understand ing of the vitamin and the cancer. With this framework in mind, this project has developed and assayed a series of B_{12}-based imaging agents for both *in vitro* and *in vivo* applications. A water soluble B_{12}-Re(I) probe that incorporated the thiazolate linker-chelator moiety was used to demonstrate the presence of cubilin in A549 lung cancer cells. A B_{12}-^{64}Cu probe was also developed and shown to selectively target tumor cells through TCII receptors in a mouse model.

My findings show that B_{12}-based bioprobes have great promise for penetrating certain cancer cell lines *in vitro*—opening up certain pathways for study for the first time. These remarkable B_{12} bioprobes developed here also target tumors selectively as imaging agents for use *in vivo.* Together, these discoveries confirm the versatility and strong potential of B_{12} bioprobes for highlighting cancers, including the often-elusive metastatic cancers that are so problematic in the clinic.

Future research will focused on refining the models presented as opposed to developing other probe constructs with varying ligands. The *in vitro* B_{12}-based probe can be modified to improve the signal-to-noise ratio in confocal microscopy

for *in vitro* assays by incorporating a lanthanide metal optimized for phosphorescence in place of the weakly fluorescent rhenium complex. The ^{64}Cu radiolabeled probe can be improved in terms of its targeting availability by using B_{12} derivatives that exclusively bind to HC. As opposed to the widely expressed TCII receptors in other tissues, HC provides a better target because there is no membrane-bound HC on noncancerous tissues.

On a cellular level, these compounds can be applied to research questions in regards to the binding of B_{12} to its transport proteins and receptors, the localization and fate of B_{12} internalized in the cell, and the molecular features that distinguish cancer cells from normal cells. The *in vivo* use of these probes allows for a greater understanding of B_{12} on the level of the organism, opening up deeper questions into the differential expression of B_{12} uptake receptors in varied tissue types, as well as the mechanisms of B_{12} storage, clearance, and recycling in the body. Overall, the work presented in this capstone addresses the needs of the research and medical communities for probes, which have a future as tools to better understand the specific biochemistry of B_{12}, the physiology of cancer, and how these two fields of study overlap to produce an interdisciplinary solution to a critical health problem.

The broad implications of these findings are further underscored by our ability to chemically modify the B_{12} molecule, the ligand, and the metal, which lends us a great deal of flexibility for future development. Hence thesee probes

can be adapted for specific experiments and research questions across an exceptionally broad span of fields, including gastroenterology, oncology, cell biology, microbiology, and organometallic chemistry. Probes that can detect cancer far earlier and more reliably are of tremendous significance for improving outcomes of this most challenging and devastating group of diseases.

References

1. Waibel, R.; Treichler, H.; Schaefer, N.G.; van Staveren, D.R.; Mundwiler, S.; Kunze, S.; Kuenzi, M.; Alberto, R.; Nuesch, J.; Knuth, A.; Moch, H.; Schibli, R.; Schubiger, PA. New Derivatives of Vitamin B_{12} Show Preferential Targeting of Tumors. *Cancer Res.* **2008**, *68*, 2904-2911.

2. Pathare, P. M.; Wilbur, D.S.; Heusser, S.; Quadros, E.V.; McLoughlin, P.; Morgan, A.C. Synthesis of cobalamin-biotin conjugates that vary in the position of cabalamin coupling. Evaluation of cabalamin derivative binding to transcoabalamin II. *Bioconjugate Chem.* **1996**, *7*, 217-232.

3. Cella, D.F.; Tulsky, D.S. Quality of life in cancer: definition, purpose, and method of measurement. *Cancer Invest.* **1993**, *11*, 327-336.

4. American Cancer Society. *Cancer Facts and Figures 2013*; American Cancer Society: Atlanta, Georgia, 2013; pp 1–64.

5. Howlader N.; Noone, A.M.; Krapcho, M., Neyman, N., Aminou, R., Altekruse, S.F., Kosary, C.L.; Ruhl, J.; Tatalovich, Z.; Cho, H.; Mariotto, A; Eisner, M.P.; Lewis, D.R.; Chen, H.S.; Feuer, E.J.; Cronin K.A. *SEER Cancer Statistics Review, 1975-2009*. National Cancer Institute. http://seer.cancer.gov/csr/1975_2009 (accessed on March 16, 2013).

6. ZurHausen, H. Papillomaviruses and Cancer: from basic studies to clinical application. *Nat. Rev. Cancer*. **2002**, *2*, 342-350.

7. Nakazawa, H.; English, D.; Randell, P.L.; Nakazawa, K.; Martel, N.; Armstrong, B.K.; Yamasaki, H. UV and skin cancer: specific p53 gene mutation in normal skin as a biologically relevant exposure measurement. *PNAS*. **1994**, *91*, 360-364.

8. Witschi H. A short history of lung cancer. *Toxicol. Sci.* **2001**, *64*, 4–6.

9. Stratton, M.R.; Campbell, P.J.; Futreal, P.A.The cancer genome. *Nature*. **2009**, *458*, 719-724.

10. Talmadge J.E.; Fidler I.J. AACR centennial series: the biology of cancer metastasis: historical perspective. *Cancer Res.* **2010**, *70*, 5649–5669.

11. Ramaswamy, S.; Ross, K.N.; Lander, E.S.; Golub, T.R. A molecular signature of metastasis in primary solid tumors. *Nature Gen.* **2003**, *33*, 49–54.

12. Coghlin, C.; Murray, G.I. Current and emerging concepts in tumour metastasis. *J. Pathol.* **2010**, *222,* 1–15.

13. Disibio, G.; French, S.W. Metastatic patterns of cancer: results from a large autopsy study. *Arch Pathol Lab Med*. **2008**, *132*, 931–939.

14. National Academy of Sciences. Institute of Medicine. Food and Nutrition Board., ed. **1998**. "Chapter 9 - Vitamin B_{12}."

15. Stubbe, J. Binding site revealed of nature's most beautiful cofactor. *Science.* **1994**, *266,*1663-1664.

16. Brink, C.; Hodgkin, D.C.; Lindsey, J.; Pickworth, J.; Robertson, J.R.; White, J.G. The crystal structure of the hexacarboxylic acid derived from B_{12} and the molecular structure of the vitamin. *Nature*. **1955**, *176*, 325-328.

17. Wang, X.; Wei, L.; Kotra, L.P. Cyanocobalamin (vitamin B_{12}) conjugates with enhanced solubility. *Bioorg. Med. Chem.* **2007**, *15*, 1780-1787.

18. Nielsen M.J.; Rasmussen, M.R.; Andersen, C.B.; Nexø, E.; Moestrup, S.K. Vitamin B_{12} transport from food to the body's cells--a sophisticated, multistep pathway. *Nat. Rev. Gastroenterol. Hepatol*. **2012**, *9*, 345-54.

19. Stabler, S.P.; Allen, R.H. Vitamin B_{12} deficiency as a worldwide problem. *Annu. Rev. Nutr.* **2004**, *24*, 299-326.

20. Baik, H.W.; Russell, R.M. Vitamin B_{12} deficiency in the elderly. *Annu. Rev. Nutr.* **1999**, *19*, 357-77.

21. Park, H. J.; Kim, J. Y.; Jung, J. I.; Kim, T.J. Characterization of a Novel Gene in the Extended MHC Region of Mouse, NG29/Cd320, a Homolog of the Human CD320. *Immune. Netw.* **2009**, *9*, 138-146.

22. Amagasaki, T.; Green, R.; Jacobsen, D.W. Expression of transcobalamin II receptors by human leukemia K562 and HL-60 cells. *Blood.* **1990**, *76,* 1380-1386.

23. Spingler, B.; Mundwiler, S.; Ruiz-Sanchez, P.; van Staveren, D.R.; Alberto, R. Vitamin B_{12} for targeted cytotoxic drug delivery *Eur. J. Inorg. Chem.* **2007**, 2641-2647.

24. Fedosov, S.N.; Grissom, C.B.; Fedosova, N.U.; Moestrup, S.K.; Nexø, E.; Petersen, T.E. Application of a fluorescent cobalamin analogue for analysis of the binding kinetics. A study employing recombinant human transcobalamin and intrinsic factor. *FEBS J*. **2006**, *273*, 4742-4753.

25. Bartholomä, M. D.; Louie, A. S.; Valliant, J. F.; Zubieta, J. Technetium and gallium derived radiopharmaceuticals: comparing and contrasting the

chemistry of two important radiometals for the molecular imaging era. *Chem. Rev*. **2010**, *110*, 2903.

26. Viola-Villegas, N.; Rabideau, A. E.; Bartholoma, M.; .Zubieta , J.; Doyle, R.P. Targeting the cubilin receptor through the vitamin $B_{(12)}$ uptake pathway: cytotoxicity and mechanistic insight through fluorescent Re(I) delivery. *J. Med. Chem*. **2009**, *52*, 5253.

27. Vortherms, A. R.; Kahkoska, A. R.; Rabideau, A. E.; Zubieta, J.; Andersen, L. L.; Madsen, M.; Doyle, R. P. A water soluble vitamin B_{12}-Re(I) fluorescent conjugate for cell uptake screens: use in the confirmation of cubilin in the lung cancer line A549. *Chem. Commun.* **2011**, *47*, 9792-9794.

28. Lee, M.; Grissom, C.B. Design, synthesis, and characterization of fluorescent cobalamin analogues with high quantum efficiencies. *Org Lett*. **2009**, *11*, 2499.

29. Neumann, M.; Detlef, G. Simple method for reduction of autofluorescence in fluorescence microscopy. *J. Histochem. Cytochem*. **2002**, *50*, 437-439.

30. Reynolds, A.; Sculimbrene, B.; Imperiali, B. Lanthanide-binding tags with unnatural amino acids: sensitizing Tb3+ and Eu3+ luminescence at longer wavelengths. *Bioconjugate Chem.* **2008**, *19*, 588-591.

31. Alessio, M.; Kinahan, P.E.; Cheng, P.M.; Vesselle, H.; Karp, J.S. PET/CT scanner instrumentation, challenges, and solutions. *Radiol. Clin. North Am.* **2004**, *42,* 1017-1032.

32. Smith, S. V. Molecular imaging with copper-64. *J. Inorg. Biochem.* **2004**, *98*, 1874-1901.

33. Wadas, T. J.; Wong, E.H.; Weisman, G.R.; Anderson, C.J. Coordinating Radiometals of Copper, Gallium, Indium, Yttrium and Zirconium for PET and SPECT Imaging of Disease. *Chem. Rev*. **2010,** *110*, 2858.

34. Boswell, C. A.; Sun, X.; Niu, W.; Weisman, G. R.; Wong, E. H.; Rheingold, A. L.; Anderson, C. J. Comparative in vivo stability of copper-64-labeled cross-bridged and conventional tetraazamacrocyclic complexes. *J. Med. Chem.* **2004,** *47*, 1465-1474.

35. Hogenkamp, H.P.C.; Collins, D.A.; Live, D.; Benson, L.M.; Naylor, S. Synthesis and characterization of nido-carborane-cobalamin conjugates. *Nucl. Med. Biol.* **2000**, *27*, 89.

36. Marques, H.M.; Scooby, D.H. Optimisation of the preparation and purification of three monocarboxylic acid derivatives of vitamin B_{12} and their characterisation by ^{13}C NMR. *Inorganica Chimica Acta.* **1989***, 162*, 151-155.

37. Davidson, M.W.; Herman, B.; Lippinscott-Schwartz, J. "Fluorophores for Confocal Microscopy."*OlympusFluoView Resource Center*. Olympus Corporation, 2009.

38. Neumann, M.; Detlef, G. Simple method for reduction of autofluorescence in fluorescence microscopy. *J. Histochem. Cytochem*. **2002,** *50*, 437-439.

39. Parker, C. A. Photoluminescence of Solutions. Elsevier, Amsterdam. **1968**.

40. IUPAC.Compendium of Chemical Terminology, 2nd ed. (the "Gold Book"). Compiled by A. D. McNaught and A. Wilkinson. Blackwell Scientific Publications, Oxford. **1997**. http://goldbook.iupac.org (accessed March 16, 2013)

41. Horrocks, W.D.; Sudnick, J.D.S. Spectroscopic Investigations of Lanthanide Ion Binding to Nucleic Acids. *J. Am. Chem. Soc.* **1979**, *101*, 334.

42. deSilva, A.P.; Gunaratne, H.Q.N.; Gunnlaugsson, T.; Huxley, A.J.M.; McCoy, C.P.; Rademacher, J.T.; Rice, T.E. Signaling Recognition Events with Fluorescent Sensors and Switches. *Chem. Rev.* **1997**, *97*, 1515.

43. Bunzli, J.C.G.; Piguet, C., Taking advantage of luminescent lanthanide ions. *Chem. Soc. Rev.* **2005**, *34*, 1048.

44. Leonard, J. P.; Nolan, C. B.; Stomeo, F.; Gunnlaugsson, T. Photochemistry and Photophysics of Coordination Compounds: Lanthanides" *Top. Curr. Chem.* **2007,** *281*, 1-43. (Invited Chapter: Eds. V. Balzani and S. Campagna).

45. "Using Synergy HT Multi-Mode Microplate Reader to Measure Time-Resolved Fluorescent Compounds." *Technical Notes*.Biotek, 29 Oct. 2002. Web. 21 Apr. 2012. <http://www.biotek.com/resources/articles/time-resolved-fluorescent-compounds.html>.

46. Gunnlaugsson, T.; Leonard, J.P.; Senechal, K.; Harte, A. J. pH responsive Eu(III)-phenanthroline supramolecular conjugate: novel "off-on-off" luminescent signaling in the physiological pH range. *J Am. Chem. Soc.* **2003,** *125*, 12062. (redrawn)

47. Parker, D.; Dickins, R.S.; Puschmann, H.; Cossland, C.; Howard, J.A.K. Being excited by lanthanide coordination complexes: aqua species, chirality, excited-state chemistry, and exchange dynamics. *Chem. Rev.* **2002,** *102*, 1977-2010.

48. Parker, D.; Beeby, A.; Williams, J.A. G. Photochemical investigations of functionalised 1,4,7,10-tetraazacyclododecane ligands incorporating naphthylchromophores. *J. Chem. Soc., Perkin Trans 2.* **1996**, 1565.

49. Parker, D.Luminescent lanthanide sensors for pH, PO_2 and selected anions. *Coordin. Chem. Rev.* **2000**, *205*, 109.

50. Gunnlaugsson, T.; Leonard, J. P. Responsive lanthanide luminescent cyclen complexes: from switching/sensing to supramolecular architectures. *Chem. Commun.* **2005**, *25,* 3114-3131.

51. McMahon, B.; Mauer, P.; McCoy, C.P.; Clive Lee, T.; Gunnlaugsson, T. Selective imaging of damaged bone structure (microcracks) using a targeting supramolecular Eu(III) complex as a lanthanide luminescent contrast agent. *J. Am. Chem. Soc.* **2009**, *131*, 17542-17543.

52. Bornhop, D.J.; Griffin, J.M.M.; Goebel, T.S.; Sudduth, M.R.; Bell, B.; Motamedi, M. Luminescent lanthanide chelate contrast agents and detection of lesions in the hamster oral cancer model. *Appl. Spect.* **2003**, *57*, 1216-1222.

Summary of Capstone Project

The National Cancer Institute (NCI) estimated that ~ 1.5 million Americans were diagnosed with cancer in 2012 and more than 0.5 million died, making cancer the second leading cause of death in the US.[1] Based on rates from 2007-2009, 41.24% of men and women born today will be diagnosed with a form of cancer at some point during their lifetime.[2]

However, trends in epidemiology reflect advances in the field that have allowed physicians to diagnose and treat cancer more effectively; the five-year relative survival rate for all cancers diagnosed between 1999 and 2005 increased 50% from the same rate in 1975-1977.[1] The NCI emphasizes that finding cancer at its most treatable stage gives patients the greatest chance of recovery.[1] Currently, tumors are most detected blood-work, X-rays, computed tomography scans, magnetic resonance imaging scans, and positron emission tomography scans.[3] Novel imaging agents that target primary and metastasized tumors offer hope for improved prognoses in the future, and there is still a great need for enhanced methods of detection, early or otherwise.

My research has been aimed at synthesizing imaging agents that selectively target tumor cells through specific receptors for vitamin B_{12} (B_{12}). B_{12}

---

[1] American Cancer Society. *Cancer Facts and Figures 2012*; American Cancer Society: Atlanta, Georgia, 2012; pp 1–64.
[2] Howlader N.; Noone, A.M.; Krapcho, M., Neyman, N., Aminou, R., Altekruse, S.F., Kosary, C.L.; Ruhl, J.; Tatalovich, Z.; Cho, H.; Mariotto, A; Eisner, M.P.; Lewis, D.R.; Chen, H.S.; Feuer, E.J.; Cronin K.A. *SEER Cancer Statistics Review, 1975-2009*. National Cancer Institute. http://seer.cancer.gov/csr/1975_2009 (accessed on March 16, 2013).
[3] Talmadge JE, Fidler IJ. AACR centennial series: the biology of cancer metastasis: historical perspective. *Cancer Research* 2010; 70(14):5649–5669.

is essential for cellular metabolism, growth, and division, and all living cells require B_{12} for survival.[4] B_{12} based probes, which exploit the supply route of B_{12} in order to target regions of extreme cell growth, are also ideal due to the low toxicity and high water solubility of the vitamin.[4]

Mammalian cells are unable to synthesize B_{12}, and it must be obtained through diet. The human body has developed a complex dietary uptake system based on soluble transport proteins in the mouth, stomach, intestine, and circulatory system.[5] The two main proteins of interest as it pertains to this research are haptocorrin (HC), which binds to B_{12} and B_{12} analogues in the mouth, stomach and blood serum, and transcobalamin II (TCII), the circulatory transport protein that facilitates B_{12} cellular entry and blood-brain barrier passage.[6]

The hypothesis of this research is that the B_{12} pathway can be exploited to offer a tropism for cancer cells; certain cell lines over-express uptake receptors for TCII (CD320 receptors) in order to meet the increased B_{12} demands of rapid and uncontrolled growth. In addition, it was recently discovered that some cell lines, like those of pancreatic cancer, express membrane-bound HC *de novo*.[1] This HC

---

[4] Waibel, R.; Treichler, H.; Schaefer, N.G.; van Staveren, D.R.; Mundwiler, S.; Kunze, S.; Kuenzi, M.; Alberto, R.; Nuesch, J.; Knuth, A.; Moch, H.; Schibli, R.; Schubiger, PA. *Cancer Res*. **2008**, 68, 2904-2911.

[5] Pathare, P. M.; Wilbur, D.S.; Heusser, S.; Quadros, E.V.; McLoughlin, P.; Morgan, A.C. *Bioconjugate Chem*. **1996,** 7, 217-232.

[6] Nielsen M.J.; Rasmussen, M.R.; Andersen, C.B.; Nexø, E.; Moestrup, S.K. Vitamin B_{12} transport from food to the body's cells--a sophisticated, multistep pathway. *Nat. Rev. Gastroenterol. Hepatol*. **2012**, *9*, 345-54.

finding has great potential for a more specific targeting of cancer cells. I have worked to synthesize, characterize and assay a series of B_{12}-based imaging agents for both *in vitro* and *in vivo* applications: a fluorescent B_{12}-based probe with which to screen cell lines for receptor targets, and also a radiolabelled B_{12}-based system to translate this work to living organisms.

For *in vitro* cancer cell screens to study uptake and localization of B_{12} conjugates, I helped to build, purify, and characterize an optimized B_{12}-based rhenium I (Re(I)) probe. A fluorescent B_{12}-based probe is useful because it allows for preliminary screening of living cells to confirm the presence of certain receptors that are important in the B_{12} uptake pathway, such as cubilin. For lab groups that are studying the differential expression of these receptors in varied tissues, such a construct provides a confirmation of the receptor functionality that cannot be obtained from genetic methods such as RT-PCR or western Blot. I synthesized, purified, and characterize a B_{12}-thiazole-Re(I) (**1**), which incorporated a bifunctional thiazole ligand that chelates the Re(I) and links to the B_{12} molecule. We showed that **1**, bound to the intestinal transport protein for B_{12} termed intrinsic factor, was internalized by lung cancer cells, which reveals its great potential as a method of screening living cell lines for the cubilin receptor and suggests the possibility of targeting drugs to lung cancer cells by aerosolizing B_{12}-drug conjugates. These results were published in *Chemical Communications*, 2011, 47, 9792-9794, in a paper titled “A water soluble vitamin B_{12}-Re(I)

fluorescent conjugate for cell uptake screens: use in the conformation of cubilin in the lung cancer line A549."[7]

However, **1** and other B_{12}Re(I) probes were limited by complications of working with Re(I). We subsequently hypothesized that replacing the rhenium metal with a lanthanide metal along with a suitable sensitizing chromophore would result in a more optimized fluorescent system. As *in vitro* imaging agents, the lanthanides (LnIII) offer long wavelength emissions and relatively long-lived excited states (milliseconds).[8] The delayed fluorescence allows the LnIII signal to be distinguished from background autofluorescence. Therefore, my second goal was to design a LnIII metal complex that maximized fluorescence and was suitable for B_{12} conjugation. To accomplish this, I traveled to Ireland to work at Trinity College, Dublin, in Professor Thorfinnur Gunnlaugsson's research group. Over the eight weeks, I designed, synthesized, and photophysically characterized a series of lanthanide complexes suitable for future B_{12} conjugation. The purification and characterization of these compounds remains as future work for the project.

For the *in vivo* imaging of tumors, and in response to the promise for copper radionuclides covalently attached to biological molecules for diagnostic imaging

---

[7] Vortherms, A. R.; Kahkoska, A. R.; Rabideau, A. E.; Zubieta, J.; Andersen, L. L.; Madsen, M.; Doyle, R. P. A water soluble vitamin B_{12}-Re(I) fluorescent conjugate for cell uptake screens: use in the confirmation of cubilin in the lung cancer line A549. *Chem. Commun.* **2011**, *47*, 9792-9794.
[8] Leonard, J. P.; Nolan, C. B.; Stomeo, F.; Gunnlaugsson, T. Photochemistry and Photophysics of Coordination Compounds: Lanthanides" *Top. Curr. Chem.* **2007,** *281*, 1-43. (Invited Chapter: Eds. V. Balzani and S. Campagna).

and targeted radiotherapy, I constructed a B_{12}-based probe by conjugating B_{12} with a linker molecule, ethylenediamine (en), and a metal-chelating macrocyclic ligand, 1,4,7,10-tetraazacyclododecane-N',N'',N''',N''''-tetraacetic acid (DOTA). The resulting compound, B_{12}enDOTA (**2**), offers a site for facile radiolabeling. **2** was purified by a two-step purification method involving an analytical anion exchange column and a C18 analytical column on reverse phase HPLC (RP-HPLC). The purity of **2** was confirmed by nuclear magnetic resonance spectrometry (^{1}H NMR) and matrix-assisted laser desorption/ionization-time of flight mass spectrometry (MALDI-TOF/ MS). In collaboration with the Washington University Medical School in St. Louis, Missouri, **2** was labeled with copper-64 (^{64}Cu) , a radioactive derivative of copper for use in positron emission topography (PET) scanning. Initial ^{64}Cu-labeling experiments were successful, showing 100% radiolabeling, the labeled analogue of **2** was tested *in vivo* in a mouse model, showing 2% tumor distribution in two different tumor models. A more stable chelator molecule, 1,4,7-triazacyclononane-*N*,*N*′,*N*″-triacetic acid (NOTA), was selected for a revised probe construct. The optimized compound B_{12}enNOTA (**3**) is expected to show a higher expected degree of kinetic stability in regards to chelating the ^{64}Cu compared to **2**. *In vivo* experiments with **3** are currently underway at Washington University.

While B_{12}-based imaging agents have experimentally labeled tumor tissue through successful receptor-mediated endocytosis of the TCII-bound B_{12}

conjugate, significant background levels of radioactivity were detected in normal tissues.[9] In particular, high uptake is seen in the kidneys and the liver because these organs are responsible for clearing and storing B_{12}, respectively. High uptake of radiolabeled compounds in the kidney may lead to radiation toxicity, and the radiation dose to the kidney is often the "dose-limiting" factor for the clinical use of nuclear medicine, and the highest expression of CD320 is seen in the kidneys, which poses a problem for the development of B_{12}-based therapeutics.[9] A solution to this problem would be to knock out the B_{12} conjugate's ability to bind with TCII, yet maintain binding with other important transport proteins. Additionally, Waibel et al. suggest that a B_{12}-based probe with decreased binding with TCII would clear from the blood more quickly than the transport protein-bound form, decreasing overall systemic toxicity.[9]

In response to the demand for a more specific imaging agent, there has been a focus on synthesizing B_{12}-based probes incorporating monocarboxylic acid derivatives of B_{12} (MCAs). It is known that mild acid hydrolysis of B_{12} produces a mixture of MCAs derived from the b-, d-, and e- propionamide side chains. While the MCAs retain vitamin function and normal interaction with HC, modification certain propionamide side chains affects B_{12}'s ability to bind with TCII, decreasing relative affinity by less than a factor of 10 for conjugates of the

[9] Waibel, R.; Treichler, H.; Schaefer, N.G.; van Staveren, D.R.; Mundwiler, S.; Kunze, S.; Kuenzi, M.; Alberto, R.; Nuesch, J.; Knuth, A.; Moch, H.; Schibli, R.; Schubiger, PA. New Derivatives of Vitamin B_{12} Show Preferential Targeting of Tumors. *Cancer Res.* **2008**, *68*, 2904-2911

b-isomer of the MCA.[10] By disrupting the binding of B_{12} to its transfer protein TCII and inhibiting uptake by TCII receptors, B_{12}–based conjugates incorporating MCAs are ideal to prevent non-targeted organ uptake and target the cancer cells that express HC *de novo* with a high signal-to-noise ratio.[10]

I have synthesized, purified, and characterized the B_{12}-monocarboxylic acids. Cyanocobalamin was reacted with 5.0M hydrochloric acid for two hours under heat (50 °C). The reaction was neutralized with 5.0M sodium hydroxide and desalted using Amberlite ion exchange resins. Purification was a two-step process, involving a cation exchange column followed by a C_{18} analytical column (HPLC). The b-, c-, and e- acids were characterized using MALDI-ToF/MS and ^{13}C NMR.

The next step is to synthesize comparable compounds of **1, 2**, and **3** utilizing the b-monocarboxylic acid derivative of B_{12}. Conjugation through the b-amide position could be used to generate a fluorescent B_{12}-MCA probe for use as a negative control in *in vitro* cell testing of B_{12}-based fluorescent probes. Because the MCAs bind only to HC, it is hypothesized that MCA-based probes will demonstrate improved *in vivo* selectivity and lower systemic toxicity. The *in vivo* probes B_{12}enDOTA and B_{12}enNOTA will be reconstructed using the *b*-MCA isomer, tested in regards to binding affinity for TCI and TCII, and evaluated on

[10] Pathare, P. M.; Wilbur, D.S.; Heusser, S.; Quadros, E.V.; McLoughlin, P.; Morgan, A.C. Synthesis of cobalamin-biotin conjugates that vary in the position of cabalamin coupling. Evaluation of cabalamin derivative binding to transcoabalamin II. *Bioconjugate Chem.* **1996,** *7*, 217-232.

animal models to compare background uptake in the kidneys and liver with the unmodified B_{12} conjugates. With such derivatives, it is expected that visualization in the PaCa-2 cells would be shut down while being increased in the B16 cells.

In conclusion, a series of B_{12}-based imaging agents were synthesized, characterized, and assayed for both *in vivo* and *in vitro* functions. A water soluble B_{12}-Re(I) probe that incorporated the thiazolate linker-chelator moiety was used to demonstrate the presence of cubilin in A549 lung cancer cells, and a B_{12}-^{64}Cu probe was shown to selectively target tumor cells through specific receptors for B_{12} in a rat model. These findings suggest that vitamin B_{12}-based bioprobes have great promise for studying the B_{12} uptake pathway in certain cancer cell lines *in vitro* and targeting tumors as imaging agents *in vivo.*

[1]Waibel, R.; Treichler, H.; Schaefer, N.G.; van Staveren, D.R.; Mundwiler, S.; Kunze, S.; Kuenzi, M.; Alberto, R.; Nuesch, J.; Knuth, A.; Moch, H.; Schibli, R.; Schubiger, PA. New Derivatives of Vitamin B12 Show Preferential Targeting of Tumors.*Cancer Res.***2008**, *68*, 2904-2911.

[2]Pathare, P. M.; Wilbur, D.S.; Heusser, S.; Quadros, E.V.; McLoughlin, P.; Morgan, A.C. Synthesis of cobalamin-biotin conjugates that vary in the position of cabalamin coupling. Evaluation of cabalamin derivative binding to transcoabalamin II.Bioconjugate Chem. **1996,***7*, 217-232.

[3]Cella, D.F.; Tulsky, D.S. Quality of life in cancer: definition, purpose, and method of measurement. *Cancer Invest.* **1993**,*11*, 327-336.

[4]American Cancer Society.*Cancer Facts and Figures 2013*; American Cancer Society: Atlanta, Georgia, 2013; pp 1–64.

[5]Howlader N.; Noone, A.M.; Krapcho, M., Neyman, N., Aminou, R., Altekruse, S.F., Kosary, C.L.; Ruhl, J.; Tatalovich, Z.; Cho, H.; Mariotto, A; Eisner, M.P.; Lewis, D.R.; Chen, H.S.; Feuer, E.J.; Cronin K.A. *SEER Cancer Statistics Review, 1975-2009*. National Cancer Institute. http://seer.cancer.gov/csr/1975_2009 (accessed on March 16, 2013).

[6]ZurHausen, H. Papillomaviruses and **cancer**: from basic studies to clinical application. *Nat. Rev. Cancer*. **2002**, *2*, 342-350.

[7]Nakazawa, H.; English, D.; Randell, P.L.; Nakazawa, K.; Martel, N.; Armstrong, B.K.; Yamasaki, H. UV and skin cancer: specific p53 gene mutation in normal skin as a biologically relevant exposure measurement. *PNAS*, **1994**, *91*, 360-364.

[8]Witschi H (2001). A short history of lung cancer.*Toxicol Sci.***64,***1*, 4–6.

[9]Stratton, M.R.; Campbell, P.J.; Futreal, P.A.The cancer genome.*Nature*.**2009**, *458*, 719-24.

[10]Talmadge JE, Fidler IJ. AACR centennial series: the biology of cancer metastasis: historical perspective. *Cancer Res.***2010.** *70*, 5649–5669.

[11]Ramaswamy, S.; Ross, K.N.; Lander, E.S.; Golub, T.R.A molecular signature of metastasis in primary solid tumors.*Nature Gen.* **2003**.*33*, 49–54.

[12]Coghlin, C.; Murray, G.I. Current and emerging concepts in tumour metastasis.*J Pathol.***2010**, *222,* 1–15.

[13]Disibio, G.; French, S.W. Metastatic patterns of cancer: results from a large autopsy study. *Arch Pathol Lab Med*. **2008**, *132*, 931–939.

[14]National Academy of Sciences.Institute of Medicine. Food and Nutrition Board., ed. (1998). "Chapter 9 - Vitamin B_{12}."

[15]Stubbe, J. Binding site revealed of nature's most beautiful cofactor. *Science.***1994,** *266,*1663-1664.

[16]Brink, C.; Hodgkin, D.C.; Lindsey, J.; Pickworth, J.; Robertson, J.R.; White, J.G. The crystal structure of the hexacarboxylic acid derived from B12 and the molecular structure of the vitamin. *Nature*.**1955**, *176*, 325-328.

[17]Wang, X., Wei, L.; Kotra, L.P. *Bioorg. Med. Chem.***2007**, *15*, 1780-87.

[18] Nielsen M.J.; Rasmussen, M.R.; Andersen, C.B.; Nexø, E.; Moestrup, S.K. Vitamin B12 transport from food to the body's cells--a sophisticated, multistep pathway. *Nat Rev GastroenterolHepatol*.**2012**, *9*, 345-54.

[19]Stabler, S.P.; Allen, R.H. Vitamin B12 deficiency as a worldwide problem.*Annu. Rev. Nutr.* **2004**, *24*, 299-326.

[20]Baik, H.W.; Russell, R.M. Vitamin B12 deficiency in the elderly *Annu. Rev. Nutr.***1999**, *19*, 357-77.

[21] Park, H. J.; Kim, J. Y.; Jung, J. I.; Kim, T.J. Characterization of a Novel Gene in the Extended MHC Region of Mouse, NG29/Cd320, a Homolog of the Human CD320. *Immune Netw.***2009,** *9*,138-146.

[22]Amagasaki, T.; Green, R.; Jacobsen, D.W. Expression of transcobalamin II receptors by human leukemia K562 and HL-60 cells.*Blood.***1990,** *76,* 1380-1386.

[23]Spingler, B.; Mundwiler, S.; Ruiz-Sanchez, P.; van Staveren, D.R.; Alberto, R. Vitamin B_{12} for targeted cytotoxic drug delivery *Eur. J. Inorg. Chem.* **2007**, 2641-2647.

[24]Fedosov, S.N.; Grissom, C.B.; Fedosova, N.U.; Moestrup, S.K.; Nexo, E.; Petersen, T.E. Application of a fluorescent cobalamin analogue for analysis of the binding kinetics. A study employing recombinant human transcobalamin and intrinsic factor.*FEBS J*. **2006**, *273*, 4742-53.

[25]Bartholomä, M. D.; Louie, A. S.; Valliant, J. F.; Zubieta, J. Technetium and gallium derived radiopharmaceuticals: comparing and contrasting the chemistry of two important radiometals for the molecular imaging era. *Chem rev*. **2010,** *110*, 2903.

[26] Viola-Villegas, N.; Rabideau, A. E.; Bartholoma, M.; .Zubieta , J.; Doyle, R.P.Targeting the cubilin receptor through the vitamin B(12) uptake pathway: cytotoxicity and mechanistic insight through fluorescent Re(I) delivery. *J. Med. Chem*., **2009**, *52*, 5253.

[27]Vortherms, A. R.; Kahkoska, A. R.; Rabideau, A. E.; Zubieta, J.; Andersen, L. L.; Madsen, M.;Doyle, R. P. A water soluble vitamin B12-ReI fluorescent conjugate for cell uptake screens: use in the confirmation of cubilin in the lung cancer line A549. *Chem. Commun.,* **2011**, *47*, 9792-9794.

[28]Lee, M.; Grissom, C.B. Design, synthesis, and characterization of fluorescent cobalamin analogues with high quantum efficiencies.*Org Lett*. **2009**, *11*, 2499.

[29]Neumann, M.; Detlef, G. Simple method for reduction of autofluorescence in fluorescence microscopy.*J HistochemCytochem.***2002,** *50*, 437-439.

[30] Reynolds, A.; Sculimbrene, B.; Imperiali, B. Lanthanide-binding tags with unnatural amino acids: sensitizing Tb3+ and Eu3+ luminescence at longer wavelengths. *Bioconjugate Chem.***2008**, *19*, 588-591.

[31]Alessio, M.; Kinahan, P.E.; Cheng, P.M.; Vesselle, H.; Karp, J.S. PET/CT scanner instrumentation, challenges, and solutions. *RadiolClin North Am.* **2004**, *42,* 1017-1032.

[32]Smith, S. V. Molecular imaging with copper-64. *J InorgBiochem.***2004**, *98*, 1874-1901.

[33]Wadas, T. J.; Wong, E.H.; Weisman, G.R.; Anderson, C.J. Coordinating Radiometals of Copper, Gallium, Indium, Yttrium and Zirconium for PET and SPECT Imaging of Disease. *Chem rev*. **2010,** *110*, 2858.

[34]Boswell, C. A.; Sun, X.; Niu, W.; Weisman, G. R.; Wong, E. H.; Rheingold, A. L.; Anderson, C. J. Comparative in vivo stability of copper-64-labeled cross-bridged and conventional tetraazamacrocyclic complexes. *J Med Chem.***2004,** *47*, 1465-1474.

[35]Hogenkamp, H.P.C.; Collins, D.A.; Live, D.; Benson, L.M.; Naylor, S. Synthesis and characterization of nido-carborane-cobalamin conjugates.*Nucl.Med. Biol.* **2000**, *27*, 89.

[36] Marques, H.M.; Scooby, D.H. Optimisation of the preparation and purification of three monocarboxylic acid derivatives of vitamin B12 and their characterisation by ^{13}C NMR. *InorganicaChimicaActa.***1989***, 162*, 151-155.

[37]Davidson, M.W.; Herman, B.; Lippinscott-Schwartz, J. "Fluorophores for Confocal Microscopy."*OlympusFluoView Resource Center*. Olympus Corporation, 2009.

[38]Neumann, M.; Detlef, G. Simple method for reduction of autofluorescence in fluorescence microscopy.*J HistochemCytochem.***2002,** *50*, 437-439.

[39]Parker, C. A. 1968.Photoluminescence of Solutions. Elsevier, Amsterdam.

[40]IUPAC.Compendium of Chemical Terminology, 2nd ed. (the "Gold Book").Compiled by A. D. McNaught and A. Wilkinson.Blackwell Scientific Publications, Oxford (1997).http://goldbook.iupac.org (accessed March 16, 2013)

[41]Horrocks, W.D.; Sudnick, J.D.S. Spectroscopic Investigations of Lanthanide Ion Binding to Nucleic Acids.*J Am. Chem. Soc.* **1979,***101*, 334.

[42]deSilva, A.P.; Gunaratne, H.Q.N.; Gunnlaugsson, T.; Huxley, A.J.M.; McCoy, C.P.; Rademacher, J.T.; Rice, T.E. Signaling Recognition Events with Fluorescent Sensors and Switches. *Chem. Rev.* **1997,***97*, 1515.

[43]Bunzli, J.C.G.; Piguet, C., Taking advantage of luminescent lanthanide ions.*Chem. Soc. Rev.* **2005,***34*, 1048.

[44]Leonard, J. P.; Nolan, C. B.; Stomeo, F.; Gunnlaugsson, T. *Top.Curr.Chem.***2007.***281*, 1.

[45] "Using Synergy HT Multi-Mode Microplate Reader to Measure Time-Resolved Fluorescent Compounds." *Technical Notes*.Biotek, 29 Oct. 2002. Web. 21 Apr. 2012. <http://www.biotek.com/resources/articles/time-resolved-fluorescent-compounds.html>.

[46]Gunnlaugsson, T.; Leonard, J.P.; Senechal, K.; Harte, A. J. pH responsive Eu(III)-phenanthroline supramolecular conjugate: novel "off-on-off" luminescent signaling in the physiological pH range. *J Am. Chem. Soc.* **2003,***125*, 12062. (redrawn)

[47] Parker, D.; Dickins, R.S.; Puschmann, H.; Cossland, C.; Howard, J.A.K. Being excited by lanthanide coordination complexes: aqua species, chirality, excited-state chemistry, and exchange dynamics. *Chem. Rev.* **2002,***102*, 1977-2010.

[48] Parker, D.; Beeby, A.; Williams, J.A. G. Photochemical investigations of functionalised 1,4,7,10-tetraazacyclododecane ligands incorporating naphthylchromophores*J. Chem Soc., Perkin Trans 2.* **1996**, 1565.

[49]Parker, D.Luminescent lanthanide sensors for pH, pO2 and selected anions.*Coordin.Chem. Rev.* **2000,***205*, 109.

[50]Gunnlaugsson, T.; Leonard, J. P. Responsive lanthanide luminescent cyclen complexes: from switching/sensing to supramolecular architectures. *Chem. Commun.* **2005**, *25,* 3114-31.

[51] McMahon, B.; Mauer, P.; McCoy, C.P.; Clive Lee, T.; Gunnlaugsson, T. Selective imaging of damaged bone structure (microcracks) using a targeting supramolecularEu(III) complex as a lanthanide luminescent contrast agent. *J. Am. Chem. Soc.* **2009**, *131*, 17542-17543.

[52]Bornhop, D.J.; Griffin, J.M.M.; Goebel, T.S.; Sudduth, M.R.; Bell, B.; Motamedi, M. Luminescent lanthanide chelate contrast agents and detection of lesions in the hamster oral cancer model. *Appl. Spect.* **2003**, *57*, 1216-1222.